Article

Potent and biostable inhibitors of the main protease of SARS-CoV-2

3 (X = O)
IC$_{50}$: 0.037 $\pm$ 0.0010 μM
EC$_{50}$: 0.29 $\pm$ 0.056 μM

Satisfactory PK profiles

4 (X = S)
IC$_{50}$: 0.37 $\pm$ 0.015 μM
EC$_{50}$: 0.34 $\pm$ 0.015 μM

Kohei Tsuji,
Takahiro Ishii,
Takuya
Kobayakawa, ...,
Shogo Misumi,
Hiroaki Mitsuya,
Hirokazu
Tamamura

tamamura.mr@tmd.ac.jp

Highlights

Potent main protease inhibitors, which block SARS-CoV-2 infection, were developed

Our strategy adopted fluorine scan and amide surrogate replacement in molecules

The antiviral activity of the top compound is higher than that of Nirmatrelvir

Some compounds have remarkably preferable pharmacokinetics in mice

iScience

Article

Potent and biostable inhibitors of the main protease of SARS-CoV-2

Kohei Tsuji,[1,9] Takahiro Ishii,[1,9] Takuya Kobayakawa,[1,9] Nobuyo Higashi-Kuwata,[2] Chika Azuma,[1]
Miyuki Nakayama,[1] Takato Onishi,[1] Hiroki Nakano,[1] Naoya Wada,[1] Miki Hori,[1] Kouki Shinohara,[1] Yutaro Miura,[1]
Takuma Kawada,[1] Hironori Hayashi,[3] Shin-ichiro Hattori,[2] Haydar Bulut,[4] Debananda Das,[4]
Nobutoki Takamune,[5] Naoki Kishimoto,[5] Junji Saruwatari,[6] Tadashi Okamura,[7] Kenta Nakano,[7] Shogo Misumi,[5]
Hiroaki Mitsuya,[2,4,8] and Hirokazu Tamamura[1,10,*]

SUMMARY

Potent and biostable inhibitors of the main protease (M^pro) of SARS-CoV-2 were designed and synthesized based on an active hit compound 5h (2). Our strategy was based not only on the introduction of fluorine atoms into the inhibitor molecule for an increase of binding affinity for the pocket of M^pro and cell membrane permeability but also on the replacement of the digestible amide bond by a surrogate structure to increase the biostability of the compounds. Compound 3 is highly potent and blocks SARS-CoV-2 infection *in vitro* without a viral breakthrough. The derivatives, which contain a thioamide surrogate in the P2-P1 amide bond of these compounds (2 and 3), showed remarkably preferable pharmacokinetics in mice compared with the corresponding parent compounds. These data show that compounds 3 and its biostable derivative 4 are potential drugs for treating COVID-19 and that replacement of the digestible amide bond by its thioamide surrogate structure is an effective method.

INTRODUCTION

The pandemic of the novel COVID-19, which is produced by the positive-strand RNA virus SARS-CoV-2, has been continuing for more than two years.[1–4] Vaccination has been pervasive worldwide and has been very effective in suppression of infection as well as aggravation, but the spread of SARS-CoV-2 has not relented because of frequent breakthrough infections in vaccinated people and the numbers of people who have avoided vaccination,[5,6] and drugs are needed to treat infected patients. Initially, Remdesivir, a repositioning inhibitor of RNA-dependent RNA polymerase (RdRp), which had been administered to patients of Ebola hemorrhagic fever, was used as the first FDA-authorized anti-COVID-19 drug.[7,8] Other inhibitors of this type, including inhibitors such as Molnupiravir,[9–11] which are specific for SARS-CoV-2 RdRp have been developed. Subsequently, Nirmatrelvir/PF-07321332 (1), aka Paxlovid, a novel inhibitor of the main protease (M^pro) of SARS-CoV-2, was authorized by FDA in 2021 (Figure 1).[12]

The genome of SARS-CoV-2 encodes two large overlapping polyproteins, pp1a and pp1ab, which are processed principally by two viral proteases, M^pro and a papain-like protease (PL^pro), to generate the virally functional proteins.[13–17] M^pro is classified as a member of the cysteine protease family. The genome of SARS-CoV-2 has approximately 80% nucleotide identity with the genome of SARS-CoV-1. The M^pros of both SARS-CoV-2 and SARS-CoV-1 have 96% amino acid sequence identity[18] and near identity in their tertiary structures and they form almost the same active center of M^pro.[19] As M^pro is essential for viral replication and there is no human enzyme closely homologous with M^pro, it is an important and attractive drug discovery target for the treatment of COVID-19. Another M^pro inhibitor, S-217622, which is apparently not correlated with covalent bond formation with M^pro, has been developed.[20] In addition, several other M^pro inhibitors have been developed to date.[21–27] As the development of additional several drugs is required for a repertory of drug choice, we have tried to develop other M^pro inhibitors. Previously, we characterized a hit compound, 5h (2), as a SARS-CoV-2 M^pro inhibitor[19] among a panel of known compounds, which had originally shown inhibitory activity against SARS-CoV (Figure 1).[28–30] As the inhibitory activity or biological stability of compound 5h (2) is insufficient, we have attempted in this study to develop more effective inhibitors with increased activity and biological stability based on compound 5h (2) and are reporting the results.

[1]Department of Medicinal Chemistry, Institute of Biomaterials and Bioengineering, Tokyo Medical and Dental University (TMDU), Chiyoda-ku, Tokyo 101-0062, Japan

[2]Department of Refractory Viral Infections, National Center for Global Health and Medicine Research Institute, Shinjuku-ku, Tokyo 162-8655, Japan

[3]Department of Infectious Diseases, International Research Institute of Disaster Science, Tohoku University, Aoba-ku, Sendai 980-8572, Japan

[4]Experimental Retrovirology Section, HIV and AIDS Malignancy Branch, National Cancer Institute, National Institutes of Health, Bethesda, MD 20892, USA

[5]Department of Environmental and Molecular Health Sciences, Faculty of Life Sciences, Kumamoto University, Chuo-ku, Kumamoto 862-0973, Japan

[6]Division of Pharmacology and Therapeutics, Graduate School of Pharmaceutical Sciences, Kumamoto University, Chuo-ku, Kumamoto 862-0973, Japan

[7]Department of Laboratory Animal Medicine, Research Institute, National Center for Global Health and Medicine, Shinjuku-ku, Tokyo 162-8655, Japan

[8]Department of Clinical Sciences, Kumamoto University Hospital, Chuo-ku, Kumamoto 860-8556, Japan

[9]These authors contributed equally

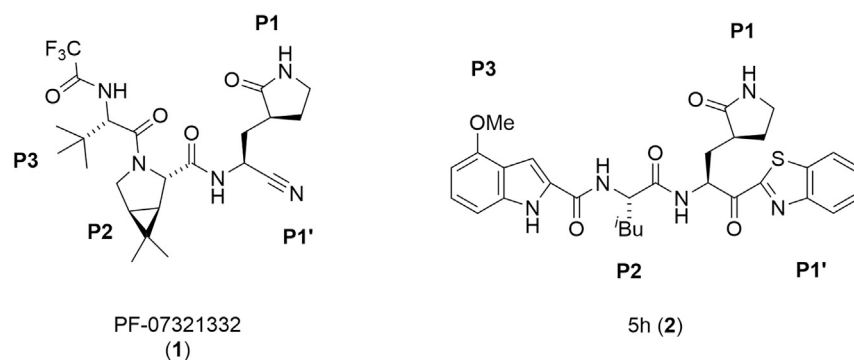[10]Lead contact

*Correspondence:
tamamura.mr@tmd.ac.jp

https://doi.org/10.1016/j.isci.2022.105365

Figure 1. The structures of SARS-CoV-2 M^pro inhibitors, Nirmatrelvir/PF-07321332 (1) and 5h (2)

RESULTS

Concept of compound design

Compound 5h (2) is a tripeptide mimic, with an electrophilic ketone group as a warhead. It functions as a tightly binding reversible-covalent inhibitor of SARS-CoV-2 and has a K_i value of 17.6 nM.[19] In common with Nirmatrelvir/PF-07321332 (1), compound 2 has P3, P2, P1, and P1' sites (Figure 1). The warhead electrophilic carbonyl group at the P1' site of compound 2 can trap the nucleophilic thiol group of Cys145 at the active center of M^pro with a reversible covalent bond, which produces a hemithioketal structure as an intermediate that can inactivate M^pro.[19,30] In order to increase the potency of M^pro inhibitors such as compound 5h (2), fluorine atoms were introduced to inhibitor molecules in an attempt to realize a fluorine-associated interaction[31] with the pocket of M^pro, and an increase of the cell membrane permeability.[32,33] To date, this fluorine scan strategy has been applied to the design of several compounds.[34–39] Practically, the effectiveness of introduction of fluorine into inhibitor molecules, including enhancement of hydrophobic interaction because of the formation of bonds between a halogen atom and the target enzyme and an increase of intracellular uptake has been revealed by the development of highly potent HIV-1 protease inhibitors.[40–42] Hydrolysis of the P1-P2 amide bond of compound 5h (2) in the liver, on the other hand might lead to its low availability.[30] Thus, the P2-P1 amide bond was replaced by a thioamide, a surrogate structure. Using a sulfur atom as an alternative to an oxygen atom, a thioamide structure is a useful biomimetic for an amide bond in natural peptides because thioamide bonds are resistant to normal peptidases, which can cleave peptide bonds.[43,44] A thioamide-containing small drug, ethionamide has been utilized as an antibiotic to treat tuberculosis for over 60 years.[45]

Synthesis of compounds 3 and 4

The purity of the final synthesized compounds was measured by analytical HPLC or NMR and was >95%. Experimental procedures of the synthesis of all of the compounds including characterization data are provided in the supplemental information – SI (Data S1). The synthesis of the representative compounds (3 and 4) is shown in Figures 2 and 3. A derivative in which the P1-P2 amide bond was replaced by thioamide, was synthesized as compound 4 (Figure 3).[46,47] Coupling of the tert-butyl ester hydrochloride of Leu (5) with 7-fluoro-4-methoxyindole-2-carboxylic acid (6) by 1-ethyl-3-(3-dimethylaminopropyl)carbodiimide (EDCI) hydrochloride, 1-hydroxybenzotriazole (HOBt) monohydrate and N,N-diisopropylethylamine (DIPEA) provided the amide (7), and this was followed by deprotection of the tert-butyl group with hydrochloride to give the acid (8). Treatment of the N^α-Boc-derivative of methyl (S)-2-amino-3-((S)-2-oxopyrrolidin-3-yl) propanoate (9) by 4-fluorobenzothiazole pretreated with n-butyllitium produced a ketone (10), and the subsequent deprotection of the N^α-Boc group with tetrafluoroboric acid diethyl ether complex gave an amine (11). Condensation of the acid (8) and the amine (11) with 1-[(1-(cyano-2-ethoxy-2-oxoethylideneaminooxy)dimethylaminomorpholino)]uronium hexafluorophosphate (COMU) in the presence of DIPEA yielded the target compound (3). Coupling of Boc-Leu-OH (12) with 4-nitro-1,2-phenylenediamine by a mixed anhydride reaction using isobutylchloroformate and N-methylmorpholine gave the amide (13). Treatment of 13 with phosphorus pentasulfide in the presence of sodium carbonate produced the thioamide (14),[46,47] and this was followed by treatment with sodium nitrite in the presence of aqueous acetic acid to yield the triazole (15). Condensation of the triazole (15) with the amine (11) in the presence of DIPEA led to a thioamide (16), and this was followed by deprotection of the N^α-Boc group
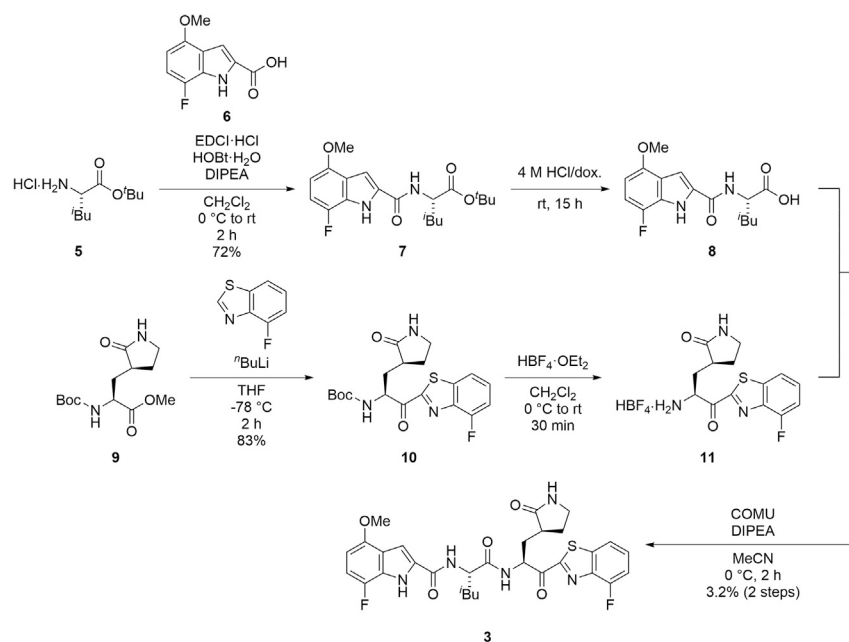
Figure 2. Synthetic scheme for compound 3

with tetrafluoroboric acid diethyl ether complex to give the amine (**17**). Condensation of the acid (**6**) with the amine (**17**) by COMU in the presence of DIPEA yielded the target compound (**4**).

Structure-activity relationship studies on derivatives modified at the P1′ site

The structure of compound 5h (**2**) is shown in Figure 1. Fluorobenzothiazolyl ketones function as a warhead with increased electrophilicity. Initially, the benzothiazole moiety at the P1′ site was modified by the introduction of fluorine atoms (Figure 4). The EC_{50} and CC_{50} values of the products were determined with RNA-qPCR and WST-8 assays, respectively, using VeroE6 cells (see the experimental model and subject details section).[19] The introduction of a fluorine atom at position 4 or 5 of the benzothiazole moiety maintained the antiviral activity (compounds **18/19**) but the introduction of a fluorine atom at position 6 (compound **20**)

Figure 3. Synthetic scheme for compound 4

Figure 4. The structures of derivatives modified at the P1′ site

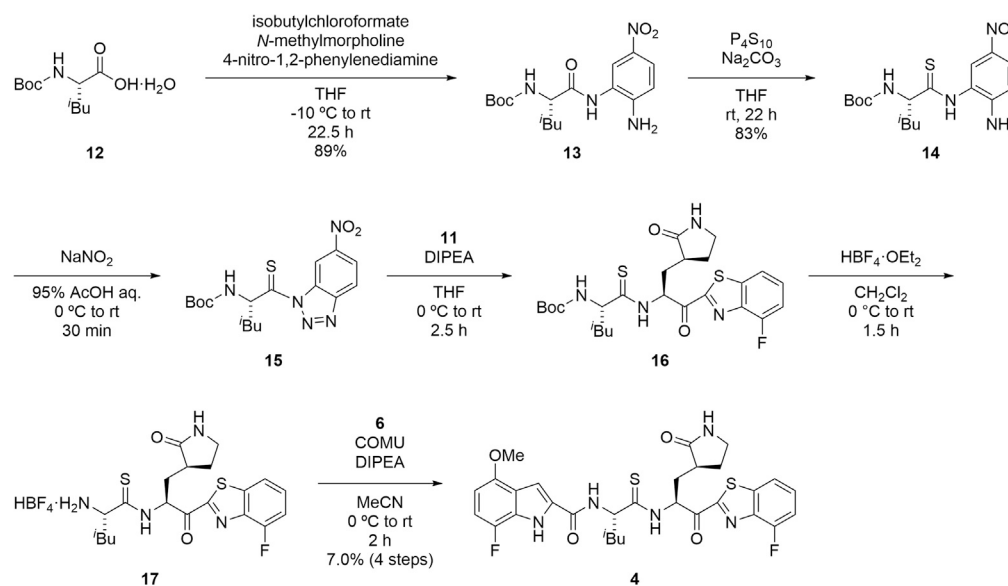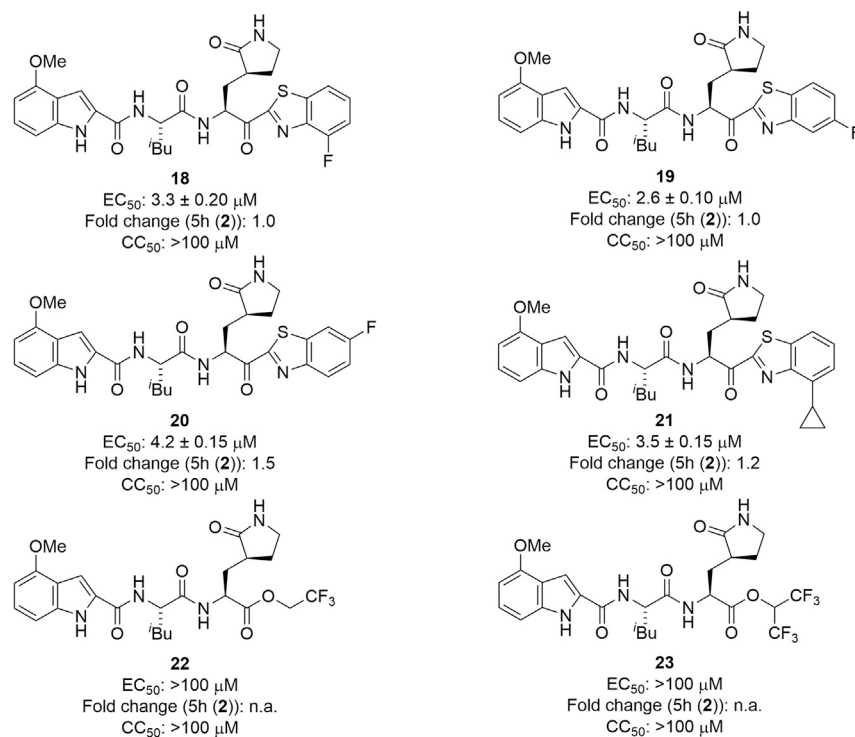EC_{50} and CC_{50} values were determined with RNA-qPCR and WST-8 assays, respectively, using VeroE6 cells.[19] The numbers represent the average EC_{50} value ± SD (μM) and CC_{50} value ± SD (μM) from at least two independent experiments. Fold changes to 5h (2) are shown. n.a., not applicable.

slightly decreased this activity. The introduction of a cyclopropane moiety at position 4 of the benzothiazole moiety gave compound **21** but did not affect the potency substantially. Derivatives bearing alkyl esters with one or two trifluoromethyl group(s) (**22** or **23**, respectively) failed to show significant antiviral activity suggesting that trifluoromethyl-containing alkyl esters when compared with those with the original benzothiazolyl ketone moiety are not suitable as units at the P1′ site. A 4- or 5-fluorobenzothiazole moiety or a normal benzothiazole moiety is suitable as a unit at the P1′ site. According to the X-ray crystal structure of M^{pro} and 5h (Figure 5B),[19] there is enough space close to position 4 or 5 of the benzothiazole moiety at the P1′ site to introduce groups such as a fluorine atom.

Structure-activity relationship studies on derivatives modified at the P3 site

Next, the indole moiety at the P3 site was modified (Figure 6). The introduction of a fluorine atom at position 7 of the indole moiety (compound **24**) maintained or slightly decreased the antiviral activity of 5h. The introduction of a fluorine atom at position 7 and the replacement of the 4-methoxy group by a fluorine atom gave compound **25**, which mostly retained the antiviral activity of 5h, indicating that the pattern of 4,7-difluoro-substituents is acceptable and that an electron-withdrawing group as well as an electron-donating group is suitable as the 4-substituent group. Other difluoro-substitutions failed to cause any positive effects: 4,5-difluoro-substitution (compound **26**) slightly decreased the antiviral activity of 5h, and 4,6-difluoro-substitution (compound **27**) largely decreased the antiviral activity of 5h. The replacement of the 4-methoxy group by a trifluoromethoxy group (compound **28**) mostly maintained the potency. According to the X-ray crystal structure of M^{pro} and 5h, there is enough space close to positions 4–7 of the indole moiety at the P3 site to introduce groups such as a fluorine atom, a methoxy group, or a trifluoromethoxy group. Positions 4–7 of the indole moiety are located in a solvent contact area (Figure 5C). The replacement of the indole moiety by a benzyloxy group (compound **29**) caused a remarkable decrease of the potency. As a result, it was concluded that 7-fluoro-4-methoxy-substituents, 4,7-difluoro-substituents, and 4-trifluoromethoxy-substituents of the indole moiety are suitable for high antiviral activity. Therefore, to perform structure-activity relationship studies on the
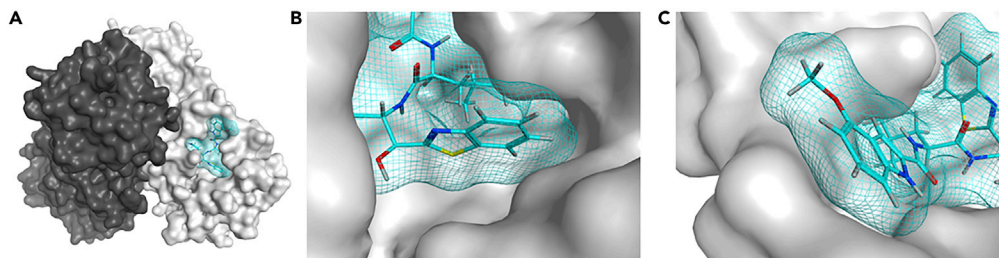
iScience
Article

CellPress
OPEN ACCESS

Figure 5. The X-ray crystal structure of SARS-CoV-2 M^pro and 5h (2) 7JKV

(A) The two protomers of SARS-CoV-2 M^{pro} are shown in black and gray surface presentations, and 5h (**2**) is shown in cyan sticks and mesh (PDB: 7JKV).[19] Hydrogen, nitrogen, oxygen, and sulfur atoms are shown in gray, blue, red, and yellow, respectively.

(B and C) The binding pocket of M^{pro}, which interacts with 5h (**2**), is shown. The benzothiazole moiety at the P1′ site is shown in the center (B). The 4-methoxyindole moiety at the P3 site, which is surrounded by hydrophobic residues, is shown in the center (C).

benzothiazole moiety, 7-fluoro-4-methoxy-substituents, 4,7-difluoro-substituents, or 4-trifluoromethoxy-substituents of the indole moiety were fixed at the P3 site.

Structure-activity relationship studies on compound 24 derivatives with a 7-fluoro-4-methoxyindole moiety at the P3 site

First, 7-fluoro-4-methoxy-substituents of the indole moiety at the P3 site were used, and the benzothiazole moiety at the P1′ site was derivatized (Figure 7). As a 4- or 5-fluorobenzothiazole moiety is suitable as a unit at the P1′ site of derivatives of 5h, which have 4-methoxyindole at the P3 site, compound **3**, which has a 4-fluorobenzothiazole moiety at the P1′ site and a 7-fluoro-4-methoxyindole moiety at the P3 site, and compound **30**, which has a 5-fluorobenzothiazole moiety at the P1′ site and a 7-fluoro-4-methoxyindole moiety at the P3 site, were designed and synthesized. Compound **3** showed remarkably higher antiviral activity than

24
EC$_{50}$: 3.4 ± 0.15 μM
Fold change (5h (**2**)): 1.2
CC$_{50}$: >100 μM

25
EC$_{50}$: 3.1 ± 0.25 μM
Fold change (5h (**2**)): 1.0
CC$_{50}$: >100 μM

26
EC$_{50}$: 4.9 ± 0.10 μM
Fold change (5h (**2**)): 1.7
CC$_{50}$: >100 μM

27
EC$_{50}$: 8.8 ± 0.25 μM
Fold change (5h (**2**)): 3.7
CC$_{50}$: >100 μM

28
EC$_{50}$: 2.9 ± 0.15 μM
Fold change (5h (**2**)): 1.0
CC$_{50}$: >100 μM

29
EC$_{50}$: 38 ± 2.5 μM
Fold change (5h (**2**)): 12
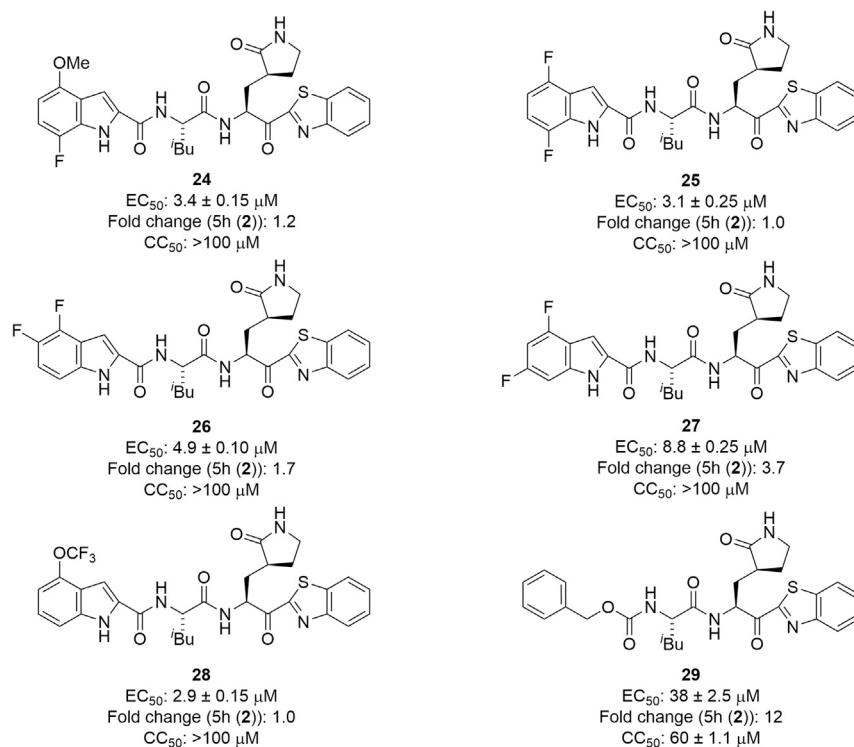CC$_{50}$: 60 ± 1.1 μM

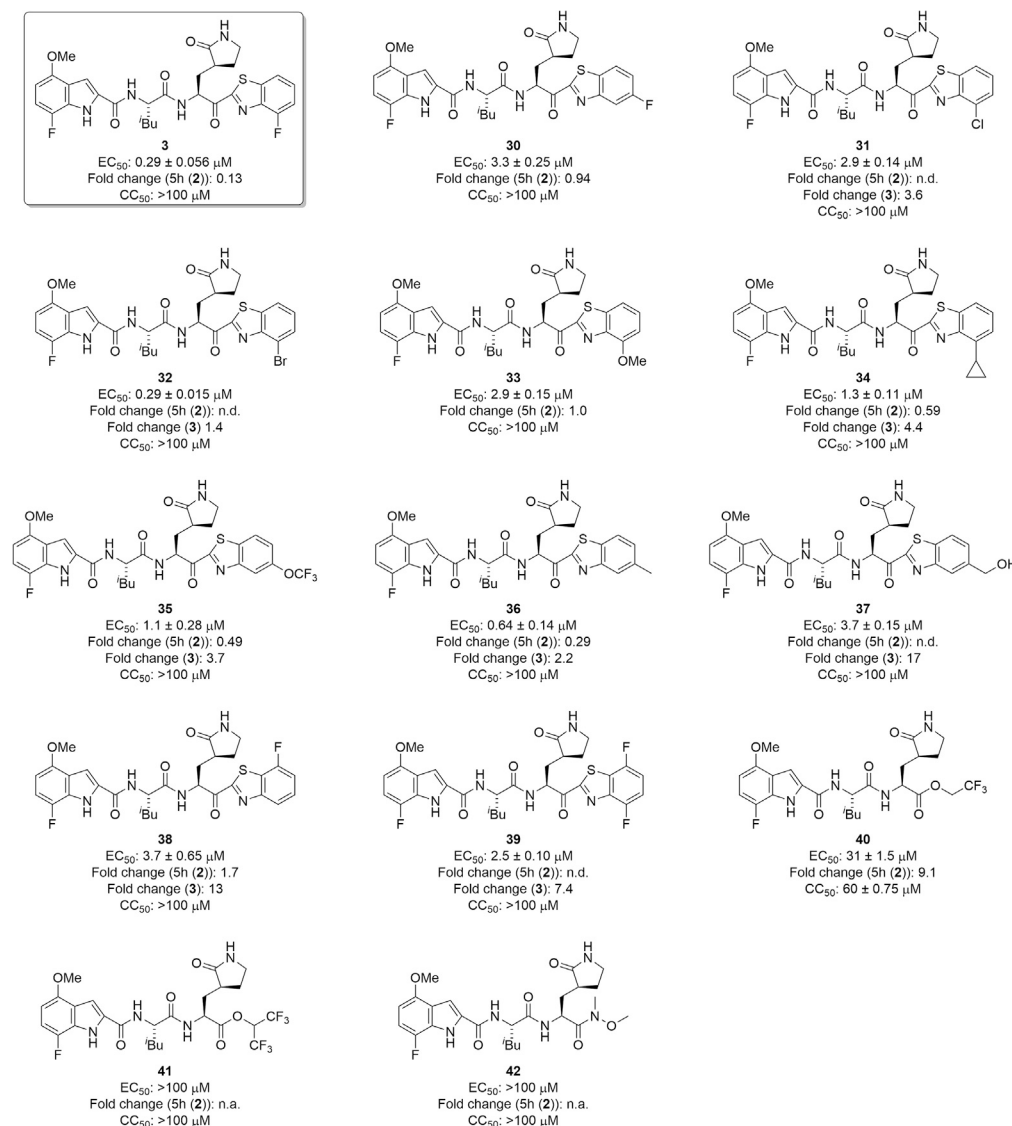**Figure 6. The structures of derivatives modified at the P3 site**

Figure 7. The structures of compound 24 derivatives with a 7-fluoro-4-methoxyindole moiety at the P3 site
n.d., not determined.

5h, and compound **30** mostly maintained the potency of 5h, suggesting that a 4-fluorobenzothiazole moiety is more suitable than a 5-fluorobenzothiazole moiety as a unit at the P1′ site. According to the X-ray crystal structure of M^{pro} and compound **3**, the complex structure of compound **3** is similar to that of 5h (Figure 8). In the complex with M^{pro}, the warhead carbonyl group at the P1′ site of compound **3**, similar to that of 5h, forms a covalent bond with the side chain thiol group of the Cys145 residue producing its hemithioketal structure, and the entire structure of compound **3** has hydrogen bond interactions as well as hydrophobic interactions with amino acid residues in the pocket of the active site. There is enough space close to positions 4 and 5 of the benzothiazole moiety at the P1′ site to introduce a fluorine atom (Figure 8A) as well as sufficient space close to positions 4–7 of the indole moiety at the P3 site to introduce a fluorine atom or a methoxy group. Positions 4–7 of the indole moiety are located in a solvent contact area (Figure 8B). Next, the replacement of the fluorine atom at position 4 of the benzothiazole moiety by a chlorine atom, a bromine atom, a methoxy group, or a cyclopropane group was investigated. Compound **24** derivatives with a 4-chlorobenzothiazole moiety, a 4-methoxybenzothiazole moiety or a 4-cyclopropylbenzothiazole moiety, (**31**, **33** and **34**, respectively) obviously decreased the potency of compound **3** but largely maintained the potency of 5h (**2**). A derivative of compound **24** with a 4-bromobenzothiazole moiety (**32**), maintained the same or slightly less potency
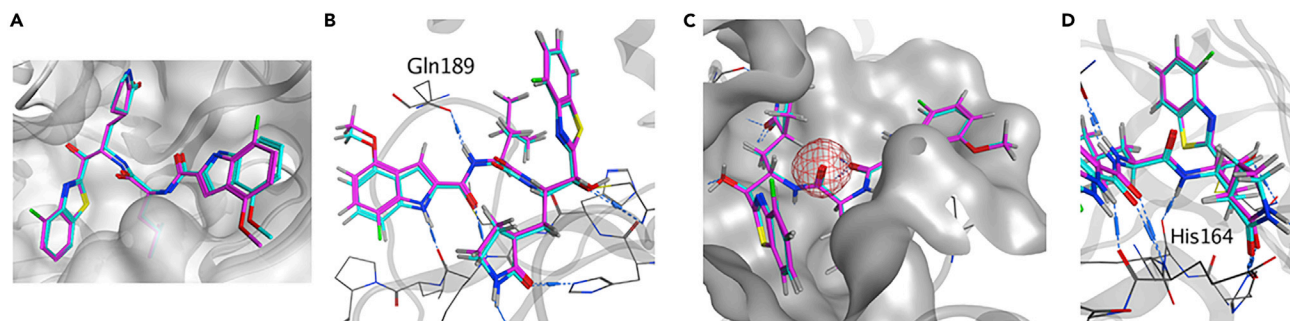
Figure 8. The superimposed structure of SARS-CoV-2 M^pro with 5h (2) (PDB: 7JKV) or compound 3 (PDB: 8DOY)

The binding pocket of M^{pro} is shown in ribbon/surface presentation in gray, and 5h (**2**) and compound **3** are shown in overlay images of cyan/magenta sticks, respectively. Hydrogen, nitrogen, oxygen, fluorine, and sulfur atoms are shown in gray, blue, red, green and yellow, respectively.

(A) The binding pocket of M^{pro}, which interacts with 5h (**2**)/compound **3**.

(B) The formation of a hydrogen bond between the N^α-amino group of L-leucine at the P2 site of 5h (**2**)/compound **3** and the sidechain carbonyl group of Gln189 is in the center.

(C) No interaction between the carbonyl group of L-leucine at the P2 site of 5h (**2**)/compound **3** (red mesh) and M^{pro} is shown in the center.

(D) The formation of a hydrogen bond between the N^α-amino group of (S)-2-amino-3-((S)-2-oxopyrrolidin-3-yl)propanoic acid at the P1 site of 5h (**2**) or compound **3** and the mainchain carbonyl group of His164 is shown in the center.

than compound **3**. In addition, the replacement of the fluorine atom at position 5 of the benzothiazole moiety of compound **30** by a trifluoromethoxy group and a methyl group was investigated. Compound **24** derivatives with a 5-trifluoromethoxybenzothiazole moiety (**35**) or a 5-methylbenzothiazole moiety (**36**) reduced the potency of compound **3**, and are more potent than compound **30**, with a 5-fluorobenzothiazole moiety. The replacement of the fluorine atom at position 5 of the benzothiazole moiety by a hydroxymethyl group was investigated. A derivative of compound **24** with a 5-hydroxymethylbenzothiazole moiety (**37**), significantly reduced the potency of compound **3**, and mostly maintained the potency of compound **30**. Judged by the X-ray crystal structure of M^{pro} with 5h (**2**) or compound **3** (Figures 5 and 7), introduction of hydrophilic groups such as hydroxymethyl at position 5 of the benzothiazole moiety is not suitable because a hydrogen bond acceptor could affect the hydrogen bond between the sidechain hydroxy group of Thr25 and the mainchain carbonyl group of Cys44 of M^{pro} and might cause the disadvantageous formation of the inhibitor-M^{pro} complex in the binding pocket. The normal benzothiazole moiety of 5h (**2**) and the 4F-benzothiazole moiety of compound **3** have no significant effect on the hydrogen bond between Thr25 and Cys44 of M^{pro} (SI, Figure S1). The 5-OCF$_3$ group on the benzothiazole ring of compound **35** plausibly forms a hydrogen bond with the sidechain hydroxy group of Thr25 and a halogen bond with the mainchain carbonyl group of Cys44 simultaneously. These interactions might contribute to a favorable formation of the inhibitor-M^{pro} complex in the binding pocket. The introduction of a fluorine atom at position 7 of the benzothiazole moiety was examined. Compound **24** derivatives having a 7-fluorobenzothiazole moiety (**38**) or a 4,7-difluorobenzothiazole moiety (**39**) showed significantly lower antiviral activity than compound **3**, which has a 4-fluorobenzothiazole moiety. This suggests that the introduction of the fluorine atom at position 7 of the benzothiazole moiety is not compatible with high potency although the introduction of the fluorine atom at position 4 is critical. The replacement of the benzothiazolyl ketone moiety by an alkylester group or an amide group was also examined. Compound **24** derivatives with alkyl esters and one or two trifluoromethyl group(s) (**40** or **41**, respectively), showed moderate or insignificant antiviral activity, indicating that trifluoromethyl-containing alkyl esters are not suitable as units at the P1′ site compared with the original benzothiazolyl ketone moiety, as has been seen in compounds **22** and **23**. A derivative of compound **24** with an added *N*-methoxy-*N*-methyl amide (a Weinreb amide) group (**42**) failed to show significant antiviral activity, suggesting that this amide group is not suitable as a unit at the P1′ site.

Structure-activity relationship studies on compound 25 derivatives having a 4,7-difluoroindole moiety at the P3 site

Next, 4,7-difluoro-substituents of the indole moiety at the P3 site were examined, and the benzothiazole moiety at the P1′ site was derivatized (Figure 9). As a 4- or 5-fluorobenzothiazole moiety is suitable as a unit at the P1′ site of 5h derivatives, compound **43**, with a 4-fluorobenzothiazole moiety at the P1′ site and a 4,7-difluoroindole moiety at the P3 site, and compound **44**, which has a 5-fluorobenzothiazole moiety at the P1′ site and a 4,7-difluoroindole moiety at the P3 site, were designed and synthesized. Compound **43**

43
EC$_{50}$: 0.40 ± 0.090 μM
Fold change (5h (**2**)): 0.18
Fold change (**3**): 1.4
CC$_{50}$: >100 μM

44
EC$_{50}$: 2.7 ± 0.15 μM
Fold change (5h (**2**)): 0.74
CC$_{50}$: >100 μM

45
EC$_{50}$: 3.2 ± 0.10 μM
Fold change (**3**): 14
CC$_{50}$: >100 μM

46
EC$_{50}$: 0.28 ± 0.010 μM
Fold change (**3**): 1.3
CC$_{50}$: >100 μM

47
EC$_{50}$: 0.50 ± 0.13 μM
Fold change (5h (**2**)): 0.22
Fold change (**3**): 1.7
CC$_{50}$: >100 μM

48
EC$_{50}$: 2.9 ± 0.20 μM
Fold change (5h (**2**)): 1.0
CC$_{50}$: >100 μM

49
EC$_{50}$: 0.79 ± 0.22 μM
Fold change (5h (**2**)): 0.36
Fold change (**3**): 2.7
CC$_{50}$: >100 μM

50
EC$_{50}$: 1.1 ± 0.20 μM
Fold change (5h (**2**)): 0.48
Fold change (**3**): 3.6
CC$_{50}$: >100 μM

51
EC$_{50}$: 24 ± 2.0 μM
Fold change (5h (**2**)): 9.8
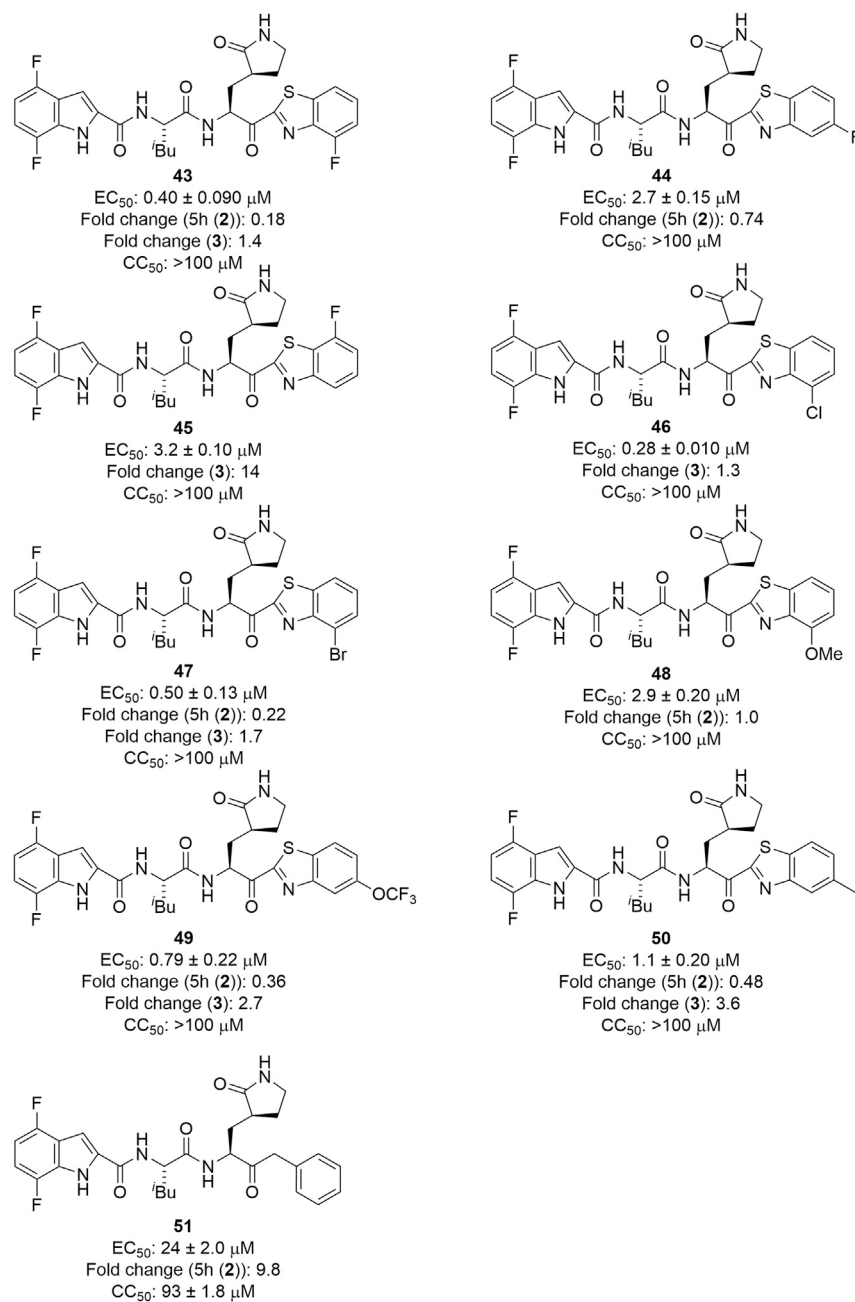CC$_{50}$: 93 ± 1.8 μM

Figure 9. The structures of compound 25 derivatives having a 4,7-difluoroindole moiety at the P3 site

showed remarkably higher antiviral activity than 5h and compound **44** showed slightly higher or equivalent potency compared with 5h, indicating that as observed in compounds **3** and **30**, a 4-fluorobenzothiazole moiety is more suitable than a 5-fluorobenzothiazole moiety as a unit at the P1′ site. The introduction of a fluorine atom at position 7 of the benzothiazole moiety was tested. A compound **25** derivative with a 7-fluorobenzothiazole moiety (**45**) showed significantly lower antiviral activity than compound **43** with a 4-fluorobenzothiazole moiety, and almost the same potency as compound **44** with a 5-fluorobenzothiazole moiety. This suggests that the introduction of a fluorine atom at position 7 of the benzothiazole moiety does not encourage high potency although the introduction of the fluorine atom at position 4 is critical. Next, the replacement of the fluorine atom at position 4 of the benzothiazole moiety by a chlorine or bromine atom or a methoxy group was investigated. Derivatives of compound **25** with
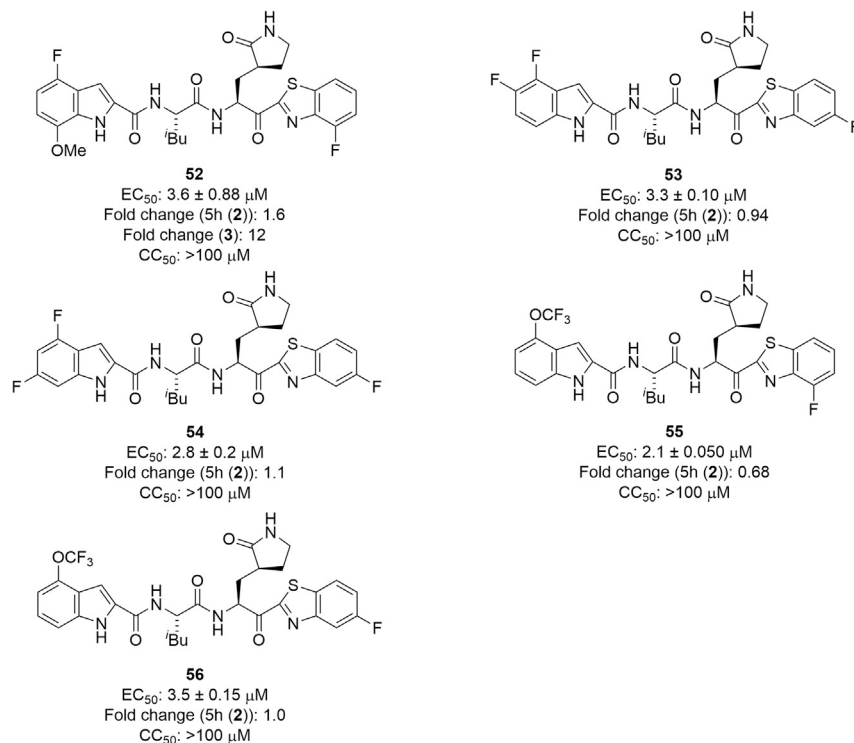
CellPress
OPEN ACCESS

52
EC$_{50}$: 3.6 ± 0.88 μM
Fold change (5h (**2**)): 1.6
Fold change (**3**): 12
CC$_{50}$: >100 μM

53
EC$_{50}$: 3.3 ± 0.10 μM
Fold change (5h (**2**)): 0.94
CC$_{50}$: >100 μM

54
EC$_{50}$: 2.8 ± 0.2 μM
Fold change (5h (**2**)): 1.1
CC$_{50}$: >100 μM

55
EC$_{50}$: 2.1 ± 0.050 μM
Fold change (5h (**2**)): 0.68
CC$_{50}$: >100 μM

56
EC$_{50}$: 3.5 ± 0.15 μM
Fold change (5h (**2**)): 1.0
CC$_{50}$: >100 μM

Figure 10. The structures of compounds with other indole derivatives at the P3 site

4-chlorobenzothiazole and 4-bromobenzothiazole moieties (**46** and **47**, respectively) mostly retained the potency of compound **43**, suggesting that a 4-chlorobenzothiazole or 4-bromobenzothiazole moiety is suitable as a unit at the P1′ site as a 4-fluorobenzothiazole moiety. A derivative of compound **25** with a 4-methoxybenzothiazole moiety (**48**) obviously reduced the potency of compound **43**, although it mostly maintained the potency of 5h, indicating that a 4-methoxybenzothiazole moiety is not suitable as a unit at the P1′ site as had been observed in compound **33**. The replacement of the fluorine atom at position 5 of the benzothiazole moiety by a trifluoromethoxy group or a methyl group was investigated. A derivative of compound **25** with a 5-trifluoromethoxybenzothiazole moiety (**49**) slightly decreased the potency of compound **43**, and is much more active than compound **44** with the 5-fluorobenzothiazole moiety, suggesting that a 5-trifluoromethoxybenzothiazole moiety is suitable as a unit at the P1′ site as observed in compound **35**. A derivative of compound **25** with a 5-methylbenzothiazole moiety (**50**) reduced the potency of compound **43**, indicating that a 5-methylbenzothiazole moiety is not suitable as a unit at the P1′ site as it is not consistent with the result observed in compound **36**. Furthermore, the replacement of the benzothiazole moiety by a benzyl group was investigated. A derivative of compound **25** with a benzyl group (**51**) showed significantly lower antiviral activity than compound **25** with a benzothiazole moiety. This suggests that a benzyl group at the P1′ site is less suitable for high potency than a benzothiazole moiety.

Structure-activity relationship studies on compounds with other indole derivatives at the P3 site

Other indole derivatives at the P3 site were investigated (Figure 10). Compound **52**, which has a 4-fluorobenzothiazole moiety at the P1′ site and a 4-fluoro-7-methoxyindole moiety at the P3 site, showed less antiviral activity than 5h, and clearly lower potency than compound **3**, which has a 7-fluoro-4-methoxyindole moiety at the P3 site. Therefore, the opposite disposition of a fluorine atom and a methoxy group as substituents on the indole moiety is unsuitable. Compound **53**, which has a 5-fluorobenzothiazole moiety at the P1′ site and a 4,5-difluoroindole moiety at the P3 site, and compound **54**, with a 5-fluorobenzothiazole moiety at the P1′ site and a 4,6-difluoroindole moiety at the P3 site, showed almost the same potency as compound **44**, which has a 5-fluorobenzothiazole moiety at the P1′ site and a 4,7-difluoroindole moiety at the P3 site. Compounds **53**, **54** and **44** showed slightly higher or equal potency as 5h, indicating that the disposition of two fluorine atoms as substituents on the indole moiety did not cause any

significant effect on antiviral activity. Compound **55**, which has a 4-fluorobenzothiazole moiety at the P1′ site and a 4-trifluoromethoxyindole moiety at the P3 site, showed almost the same antiviral activity as compound **18**, which has a 4-fluorobenzothiazole moiety at the P1′ site and a 4-methoxyindole moiety at the P3 site. Compound **56**, which has a 5-fluorobenzothiazole moiety at the P1′ site and a 4-trifluoromethoxyindole moiety at the P3 site, showed almost the same antiviral activity as compound **19**, which has a 5-fluorobenzothiazole moiety at the P1′ site and a 4-methoxyindole moiety at the P3 site. Therefore, a 4-methoxyindole moiety and 4-trifluoromethoxyindole moiety at the P3 site have almost the same effect on the potency.

Structure-activity relationship studies on derivatives, in which the L-Leucine residue at the P2 site was modified

Next, the L-leucine residue at the P2 site was modified (Figure 11) because the amide bond between the P2 and P1 sites is susceptible to hydrolysis in the liver according to the metabolic analysis of 5h performed by Konno et al.[30] N^{α}-Methylation of amino acid residues is simple and useful for modification of amide bonds. N^{α}-Methylation of (S)-2-amino-3-((S)-2-oxopyrrolidin-3-yl)propanoic acid corresponding to the P1 site is described below. Firstly, N^{α}-methyl-L-leucine corresponding to the P2 site was used to prepare compounds **57**, **58** and **59**. Compound **57** is a derivative of 5h (**2**) with N^{α}-methyl-L-leucine at the P2 site, and both compounds **57** and 5h (**2**) have a benzothiazole moiety at the P1′ site and a 4-methoxyindole moiety at the P3 site. Compound **57** shows remarkably lower antiviral activity than 5h (**2**), suggesting that N^{α}-methylation of the L-leucine residue at the P2 site does not maintain or increase the potency. According to the X-ray crystal structure of M^{pro} and 5h (**2**) or compound **3** (Figure 8B), the α-amino hydrogen atom of the L-leucine residue at the P2 site interacts with the carbonyl oxygen atom of the side chain of Gln189 of M^{pro} by hydrogen bonding. Compound **58** is a derivative of compound **30** with N^{α}-methyl-L-leucine at the P2 site, and compounds **58** and **30** both have a 5-fluorobenzothiazole moiety at the P1′ site and a 7-fluoro-4-methoxyindole moiety at the P3 site. Compound **58** showed significantly lower antiviral activity than compound **30**. This is consistent with the observation that N^{α}-methylation of the L-leucine residue at the P2 site does not maintain or increase the potency. Compound **59** is a derivative of compound **44** with N^{α}-methyl-L-leucine at the P2 site, and both compounds **59** and **44** have a 5-fluorobenzothiazole moiety at the P1′ site and a 4,7-difluoroindole moiety at the P3 site. Compound **59** mostly maintains the antiviral activity of compound **44**, but shows significant cytotoxicity and CC_{50} = 96 μM. The reason why N^{α}-methylation of the L-leucine residue at the P2 site is suitable for the maintenance of potency only in the case of compound **59** is unclear, but compound **59** is not appropriate as a lead because of its significant cytotoxicity. A thioamide structure being analogous to a carboxyamide bond, a dipeptide surrogate corresponding to the P2-P1 site, L-Leu-ψ[C(S)-NH]-(S)-2-amino-3-((S)-2-oxopyrrolidin-3-yl)propanoic acid, was synthesized and used to prepare compounds **4**, **60**, **61** and **62**. Compound **60** is a derivative of 5h (**2**) with L-Leu-ψ[C(S)-NH]-(S)-2-amino-3-((S)-2-oxopyrrolidin-3-yl)propanoic acid at the P2-P1 site, and both compounds **60** and 5h (**2**) have a benzothiazole moiety at the P1′ site and a 4-methoxyindole moiety at the P3 site. Compound **60** mostly maintained the antiviral activity of 5h. As a result, the thioamide structure of the L-leucine residue at the P2 site was deemed to be suitable for the maintenance of the potency of 5h. This suggests that, according to the X-ray crystal structure of the complex of 5h (**2**) and M^{pro} (Figure 8C), as there is no interaction between M^{pro} and the carbonyl group of the L-leucine residue at the P2 site, this carbonyl group can be changed to a surrogate such as a thiocarbonyl group. Compound **60** is appropriate as a lead compound of biostable inhibitors, and it was subjected to *in vivo* stability testing. Compounds **4**, **61** and **62** are derivatives of compounds **3**, **44** and **56**, respectively, with L-Leu-ψ[C(S)-NH]-(S)-2-amino-3-((S)-2-oxopyrrolidin-3-yl)propanoic acid at the P2-P1 site and the corresponding benzothiazole moieties at the P1′ site and indole moieties at the P3 site. The thiocarbonyl type derivatives **4**, **61** and **62** mostly maintained or enhanced the antiviral activity of the corresponding parent carbonyl compounds **3**, **44** and **56**, respectively. The replacement of the carbonyl structure of the L-leucine residue at the P2 site by a thiocarbonyl structure is also applicable in the case of compounds **3**, **44** and **56**, although compounds **61** and **62** showed significant cytotoxicity, with CC_{50} = 38 ± 1.1 μM and 50 ± 1.1 μM, respectively. Similar to compound **60**, compound **4** is appropriate as a lead compound for biostable inhibitors, and was submitted to *in vivo* stability tests. The replacement of the L-leucine residue at the P2 site by other amino acid residues was explored. Compounds **63** and **64** are a derivative of compound **30** with 1-aminocyclopentane-1-carboxylic acid and a derivative of compound **3** with 1-amino-3,3-difluorocyclopentane-1-carboxylic acid, respectively, at the P2 site, a 5- or 4-fluorobenzothiazole moiety, respectively, at the P1′ site, and a 7-fluoro-4-methoxyindole moiety at the P3 site. Compounds **63** and **64** have a remarkably reduced antiviral activity compared with compounds **30** and **3**. As a result, the
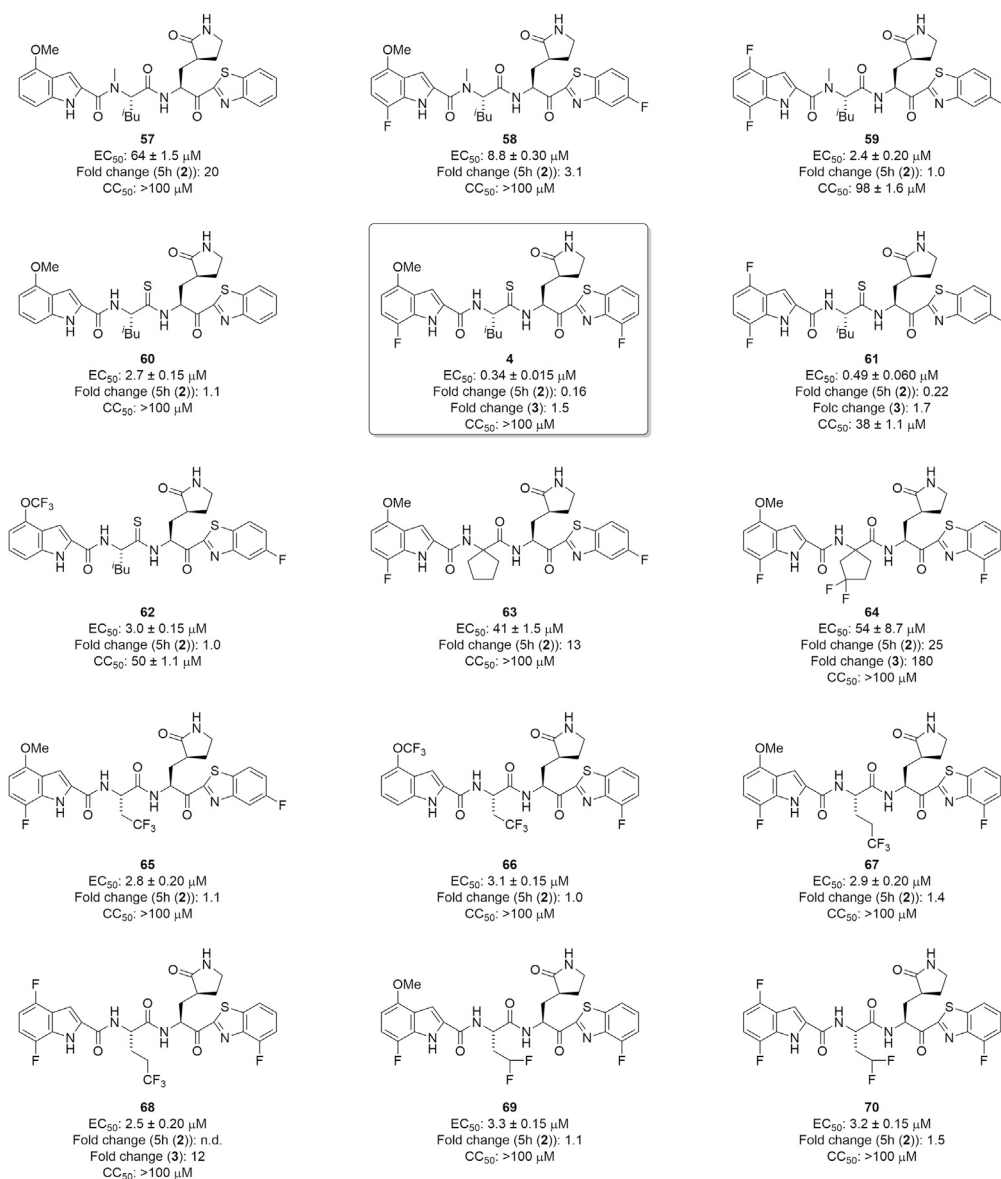
Figure 11. The structures of derivatives, in which the L-leucine residue at the P2 site was modified

substitution of a 1-aminocyclopentane-1-carboxylic acid derivative at the P2 site was deemed to be unsuitable for the maintenance of the potency of compounds **30** and **3**. Compounds **65** and **66** are derivatives of compounds **30** and **55**, respectively, with L-trifluoromethylalanine at the P2 site, the corresponding benzothiazole moieties at the P1′ site and indole moieties at the P3 site. Compounds **65** and **66** mostly retained the antiviral activity of the parent compounds **30** and **55**, respectively. The substitution of L-trifluoromethylalanine at the P2 site is applicable. Compounds **67** and **68** are derivatives of compounds **3** and **43**, respectively, with L-trifluoroethylalanine at the P2 site, the corresponding benzothiazole moieties at the P1′ site and indole moieties at the P3 site. Compounds **67** and **68** had a reduced antiviral activity of the parent compounds **3** and **43**, respectively. The substitution of L-trifluoroethylalanine at the P2 site fails to maintain the potency. Compounds **69** and **70** are derivatives of compounds **3** and **43**, respectively, with L-difluoromethylalanine at the P2 site, the corresponding benzothiazole moieties at the P1′ site and indole moieties at the P3 site. Compounds **69** and **70** have lower antiviral activity than the parent compounds **3** and **43**, respectively. In contrast to the substitution of L-trifluoroethylalanine, substitution of L-difluoromethylalanine at the P2 site fails to maintain the potency of the compound. Concerning the
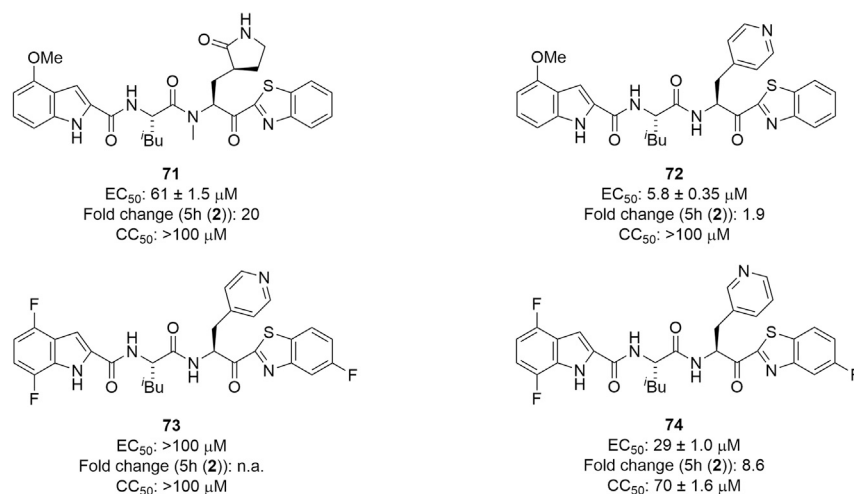
71
EC$_{50}$: 61 ± 1.5 μM
Fold change (5h (**2**)): 20
CC$_{50}$: >100 μM

72
EC$_{50}$: 5.8 ± 0.35 μM
Fold change (5h (**2**)): 1.9
CC$_{50}$: >100 μM

73
EC$_{50}$: >100 μM
Fold change (5h (**2**)): n.a.
CC$_{50}$: >100 μM

74
EC$_{50}$: 29 ± 1.0 μM
Fold change (5h (**2**)): 8.6
CC$_{50}$: 70 ± 1.6 μM

Figure 12. The structures of derivatives, in which the (*S*)-2-amino-3-((*S*)-2-oxopyrrolidin-3-yl)propanoic acid residue at the P1 site was modified

replacement of the L-leucine residue at the P2 site by other amino acid residues, the replacement by L-trifluoromethylalanine might be applicable, but the replacement by a 1-aminocyclopentane-1-carboxylic acid derivative, L-trifluoroethylalanine, or L-difluoromethylalanine is unsuitable. This suggests that considering the space between the S2 site of M^{pro} and the side chain group of the L-leucine residue at the P2 site as shown in the X-ray crystal structure of the complex of compound **3** and M^{pro}, the side chain group of L-trifluoromethylalanine might be suitable in size for the S2 site of M^{pro}, but the side chain groups of a 1-aminocyclopentane-1-carboxylic acid derivative, L-trifluoroethylalanine, and L-difluoromethylalanine are too large to fit the S2 site of M^{pro} (Figure S2).

Structure-activity relationship studies on derivatives, in which the (*S*)-2-amino-3-((*S*)-2-oxopyrrolidin-3-yl)propanoic acid residue at the P1 site was modified

Finally, the (*S*)-2-amino-3-((*S*)-2-oxopyrrolidin-3-yl)propanoic acid residue at the P1 site was modified (Figure 12). *N*^{α}-Methylation of (*S*)-2-amino-3-((*S*)-2-oxopyrrolidin-3-yl)propanoic acid corresponding to the P1 site was investigated because, as mentioned above, the amide bond between the P2 and P1 sites is susceptible to hydrolysis. Compound **71** is a derivative of 5h with *N*^{α}-methyl-(*S*)-2-amino-3-((*S*)-2-oxopyrrolidin-3-yl)propanoic acid at the P1 site, and both compounds **71** and 5h have a benzothiazole moiety at the P1′ site and a 4-methoxyindole moiety at the P3 site. Compound **71** had a significantly reduced antiviral activity compared with 5h, suggesting that *N*^{α}-methylation of the (*S*)-2-amino-3-((*S*)-2-oxopyrrolidin-3-yl)propanoic acid residue at the P1 site is not suitable for the maintenance or increase of potency. According to the X-ray crystal structure of M^{pro} and 5h (Figure 8D), the α-amino hydrogen atom of the (*S*)-2-amino-3-((*S*)-2-oxopyrrolidin-3-yl)propanoic acid residue at the P1 site enjoys hydrogen bonding with the carbonyl oxygen atom of His164 of M^{pro}. Substitution of other amino acid residues at the P1 site was examined. Compound **72** is a derivative of 5h with L-pyridin-4-ylalanine at the P1 site, and both compounds **72** and 5h have a benzothiazole moiety at the P1′ site and a 4-methoxyindole moiety at the P3 site. Compound **72** reduced the antiviral activity of 5h by about 50%. Compound **73** is a derivative of compound **44** with L-pyridin-4-ylalanine at the P1 site, and both compounds **73** and **44** have a 5-fluorobenzothiazole moiety at the P1′ site and a 4,7-difluoroindole moiety at the P3 site. Compound **73** failed to show antiviral activity below 100 μM. Compound **74** is a derivative of compound **44** with L-pyridin-3-ylalanine at the P1 site, and has a 5-fluorobenzothiazole moiety at the P1′ site and a 4,7-difluoroindole moiety at the P3 site. Compound **74** showed significantly reduced antiviral activity compared with compound **44**. This indicates that the substitution of L-pyridin-3- or 4-ylalanine at the P1 site is not applicable. The (*S*)-2-amino-3-((*S*)-2-oxopyrrolidin-3-yl)propanoic acid residue at the P1 site has been widely used in the design of human rhinovirus 3C protease inhibitors,[48] and might be indispensable.

In terms of cytotoxicity, the CC$_{50}$ values of all of the synthesized compounds, with the exception of compounds **29**, **40**, **51**, **59**, **61** and **62** are over 100 μM, suggesting absence of significant cytotoxicity.

iScience
Article

CellPress
OPEN ACCESS

Table 1. Enzymatic inhibitory activity of synthesized compounds

Compound	IC_{50} (μM)	EC_{50} (μM)	CC_{50} (μM)
5h (2)	0.36 ± 0.0050 (1.0)[a]	2.2 ± 0.53 (1.0)	>100
24	0.054 ± 0.0015 (0.15)	3.4 ± 0.15 (1.2)	>100
28	2.5 ± 0.023 (7.1)	2.9 ± 0.15 (1.0)	>100
3	0.037 ± 0.0010 (0.10)	0.29 ± 0.056 (0.026)	>100
43	0.050 ± 0.0070 (0.14)	0.40 ± 0.090 (0.2)	>100
44	0.12 ± 0.010 (0.34)	2.7 ± 0.15 (0.7)	>100
54	0.54 ± 0.020 (1.5)	2.8 ± 0.20 (1.1)	>100
60	0.99 ± 0.060 (2.8)	2.7 ± 0.15 (1.1)	>100
4	0.37 ± 0.015 (1.0)	0.34 ± 0.015 (0.16)	>100
61	0.67 ± 0.050 (1.9)	0.49 ± 0.060 (0.2)	38 ± 1.1
PF-07321332 (1)	0.028 ± 0.0050 (0.080)	1.6 ± 0.51 (0.55)	>100
Remdesivir	not tested	5.0 ± 0.050 (1.5)	>100

The inhibitory activity of each compound against M^{pro} (IC_{50} value) was determined using 3CL Protease, Untagged (SARS-CoV-2) Assay Kit (BPS Bioscience: Catalog#: 78042-1).[19]

EC_{50} values were determined with RNA-qPCR and CC_{50} values with WST-8 assays, using VeroE6 cells.

Numbers represent the average IC_{50} value ± SD (μM), EC_{50} value ± SD (μM), and CC_{50} value ± SD (μM) from two independent experiments. EC_{50} and CC_{50} values for **24, 28, 3, 43, 44, 54, 60, 4,** and **61** are from Figures 6, 7, 9, 10, and 11.

[a]The numbers in parentheses show fold changes to 5h.

Enzymatic inhibitory activity of synthesized compounds

As the antiviral activity of the synthesized compounds was evaluated against SARS-CoV-2 in VeroE6 cells and several compounds showed significant antiviral activity, enzymatic inhibitory activity of selected hit compounds against M^{pro} was investigated for target validation (Table 1) (experimental model and subject details section).[19] In most compounds, antiviral activity (EC_{50}) and enzymatic inhibitory activity (IC_{50}) are positively correlated, and the M^{pro} inhibitory activity is approximately one order greater than the antiviral activity according to IC_{50} and EC_{50} values observed with the parent compound 5h. Compound **24**, a 5h derivative with a 7-fluoroindole moiety at the P3 site, showed potent M^{pro} inhibitory activity in view of its antiviral activity whereas compound **28**, a 5h derivative with a 4-trifluoromethoxyindole moiety at the P3 site, showed low M^{pro} inhibitory activity compared with its antiviral activity, suggesting that compound **28** might easily penetrate cells and is biologically stable (see investigation of pharmacokinetics (PK)). Compound **3**, which has a 4-fluorobenzothiazole moiety at the P1′ site and a 7-fluoroindole moiety at the P3 site, compound **43**, which has a 4-fluorobenzothiazole moiety at the P1′ site and a 4,7-difluoroindole moiety at the P3 site, and compound **44**, which has a 5-fluorobenzothiazole moiety at the P1′ site and a 4,7-difluoroindole moiety at the P3 site, all showed M^{pro} inhibitory activity comparable with their antiviral activity. Compound **54**, which has a 5-fluorobenzothiazole moiety at the P1′ site and a 4,6-difluoroindole moiety at the P3 site, showed M^{pro} inhibitory activity similar to its antiviral activity. The M^{pro} inhibitory activity of the thiocarbonyl type derivatives **4, 60,** and **61** was almost equal to their antiviral activity, according to the IC_{50} and EC_{50} values. This suggests that compared with the corresponding parent carbonyl compounds **3, 5h,** and **44**, such thiocarbonyl type derivatives might show significant activity in cells relative to their enzyme inhibitory activity, possibly because of enhanced cellular penetration or biological stability. The clinically used drug Nirmatrelvir/PF-07321332 (**1**) exhibits potent M^{pro} inhibitory activity comparable with its antiviral activity. In order to confirm that the anti-SARS-CoV-2 activity of the compounds could not be because of non-specific cytotoxicity, immunostaining experiments were performed.[19] These experiments showed that compounds **3** and **4** have no significant cytotoxicity at concentrations up to 100 μM (SI, Figure S3).

Detailed antiviral activity of compounds 3 and 4 against SARS-CoV-2

The antiviral activity of the hit compounds (**3, 4**) against SARS-CoV-2 was investigated in detail (Table 2). The EC_{75} and EC_{99} values of these compounds were determined and compared with the values from 5h (**2**) and PF-07321332 (**1**). Compound **3** showed the most potent antiviral activity among the four compounds

Table 2. Detailed antiviral activity of compounds 3 and 4 against SARS-CoV-2

Compound	EC_{50} (µM)	EC_{75} (µM)	EC_{99} (µM)	CC_{50} (µM)
5h (2)	1.9 ± 0.50	4.3 ± 0.58	8.4 ± 0.23	>100
3	0.23 ± 0.030	0.46 ± 0.020	0.97 ± 0.0020	>100
4	0.28 ± 0.045	0.59 ± 0.030	4.1 ± 3.1	>100
PF-07321332 (1)	1.9 ± 0.18	4.4 ± 0.21	9.7 ± 0.015	>100

EC_{50}, EC_{75}, and EC_{99} values were determined with RNA-qPCR and CC_{50} values were determined with WST-8 assays, using VeroE6 cells.
Numbers represent the average EC_{50} value ± SD (µM) and CC_{50} value ± SD (µM) from two independent experiments.

with an EC_{99} of <1 µM. In the EC_{50}, EC_{75}, and EC_{99} values, compound **3** is superior to PF-07321332 (**1**) by approximately one order of magnitude. A thiocarbonyl type compound (**4**) also showed more potent antiviral activity than PF-07321332 (**1**) in each of these three indexes. Thus, compounds **3** and **4** are useful lead compounds as anti-SARS-CoV-2 drugs.

Antiviral activity of compound 3 against some SARS-CoV-2 mutants

Initially, we investigated the effects of the synthesized compounds against a WK-521 strain of SARS-CoV-2 (ancestral Wuhan strain),[19] which is classified into various Wuhan strains. Although M^{pro}, especially its active center, has common structures in different mutants, various SARS-CoV-2 mutants were tested in the present study (Table 3). The parent compound, 5h (**2**), showed significant antiviral activity against QHN001 (α), TY8-612 (β), TY7-501 (γ), K1734 (δ), K5356 (κ), 00012 (o, BA.1), and 02037 (o, BA.2) strains at micromolar levels when tested against a WK-521 strain, and a lead compound (**3**) exhibited approximately one order of magnitude more potent antiviral activity than 5h (**2**) against these mutant strains. This universal effectivity is an impactful advantage of compound **3**.

Investigation of pharmacokinetics (PK)

The pharmacokinetics of synthesized compounds PF-07321332 (**1**), 5h (**2**), **24**, **28**, **60**, **44**, **3**, **43**, and **4** in mice were investigated. Compounds PF-07321332 (**1**), 5h (**2**), **24**, **28**, **60**, **44**, **3**, **43**, and **4** were administered intravenously (i.v.) at 2.0 mg/kg into mice. Blood samples were collected at various time points after administration (15, 30, 60, 120, and 240 min) and the plasma was obtained by centrifugation. All of the compounds were detected by LC-MS/MS. (Figures 13A and 13B). The half-life values were calculated using a noncompartment model (for details, see the experimental model and subject details section) (Figure 13E). As a result, the half-life values of PF-07321332 (**1**) and 5h (**2**) were <23 min, relatively shorter than those of the other compounds. The half-life values of compounds **24** and **44** (∼30 min) were also short, suggesting that the introduction of fluorine atoms in the indole moiety at the P3 site might not significantly extend the half-life. The half-life values of compounds **28** and **60** (∼50–60 min) are approximately 2–3 times longer than that of the parent compound, indicating that the introduction of a 4-trifluoromethoxy group in the indole moiety at the P3 site and the replacement of the P2-P1 amide bond by a thioamide structure might prolong the half-life. High blood concentrations of compound **60** were maintained after 60 min, and even 240 min had passed. The positive effect of the thioamide structure of compound **60** is reasonable because hydrolysis of the P2-P1 amide bond of 5h (**2**) with human and rat cryopreserved hepatocytes might underlie its low biological stability.[30] The positive effect of the 4-trifluoromethoxy group in the indole moiety at the P3 site of compound **28** is also reasonable because metabolism of the 4-methoxy group of 5h (**2**) with cryopreserved hepatocytes, producing a hydroxyl group was detected.[30] The half-lives of potent compounds **3**, **4** and **43** (32–37 min) were also short, suggesting the introduction of fluorine atoms in the benzothiazole moiety at the P1' site as well as in the indole moiety at the P3 site might not significantly prolong the half-life, and that the replacement of the P2-P1 amide bond of compound **3** by a thioamide structure did not have any significant effect on prolongation of the half-life although higher blood concentrations of compound **4** were maintained compared with those of compound **3** after 60 min, and even 240 min. Compounds **3**, **4**, and **28**, which showed relatively satisfactory PKs upon i.v. administration, were administered orally (p.o.) at 2.00 mg/kg and intraperitoneally (i.p.) at 20 mg/kg into mice. Blood samples were collected at various time points after administration (15, 30, 60, 120, 240, 480 and 1,440 min) (Figures 13C, 13D and 13F). Although the half-life of compound **4** after p.o. administration (2.85 h) was

iScience
Article

CellPress
OPEN ACCESS

Table 3. Antiviral activity of compound 3 against some SARS-CoV-2 mutants

Strains	5h (2) EC_{50} (µM)	3 EC_{50} (µM)
WK-521 (ancestral Wuhan strain)	2.6 ± 0.070	0.28 ± 0.02
QHN001 (α)	2.3 ± 0.090	0.34 ± 0.09
TY8-612 (β)	2.2 ± 0.050	0.22 ± 0.035
TY7-501 (γ)	2.4 ± 0.050	0.28 ± 0.060
K1734 (δ), Exp. 1	2.7 ± 0.075	0.35 ± 0.15
K1734 (δ), Exp. 2	not tested	0.59 ± 0.24
K5356 (κ)	2.4 ± 0.13	0.29 ± 0.065
00012 (o, BA.1)	Not tested	0.47 ± 0.050
02037 (o, BA.2)	Not tested	0.33 ± 0.10

EC_{50} values were determined with RNA-qPCR and CC_{50} values with WST-8 assays, using VeroE6 cells.
Numbers represent the average EC_{50} value $\pm$ SD (µM) and CC_{50} value $\pm$ SD (µM) from two independent experiments.
Exp.: experiment.

shorter than that of compound **3** (4.33 h), compound **4** maintained remarkably higher blood concentrations for the first day than compound **3**. The initial concentration of compound **3** did not increase compared with that of compound **4**, and a relatively higher value of the half-life of compound **3** was calculated. The half-life value of compound **4** after i.p. administration (3.84 h) was longer than that of compound **3** (2.72 h), and compound **4** maintained remarkably higher blood concentrations than compound **3**, although after 1 day, the concentration of compound **3** was slightly higher than that of compound **4**. In p.o. and i.p. administrations, the replacement of the P2-P1 amide bond of compound **3** by a thioamide structure might effectively extend the half-life. The PK profiles of compound **28** in p.o. and i.p. administrations were not satisfactory when compared with those of compound **4**. As a result, the replacement of the P2-P1 amide bond of these inhibitors by a thioamide structure was thought to possibly lead to favorable PK profiles. Although compounds **28** and **60** are suitable compounds in i.v. administration, taken together with antiviral activity compound **4** is a more suitable compound, particularly when administered p.o. or i.p.

DISCUSSION

As the development of new drugs in addition to existing drugs is necessary to support a repertory of chemotherapeutic choice, we attempted to develop novel M^{pro} inhibitors based on a previously characterized compound, 5h (**2**). In this study we developed more effective inhibitors with increased activity and biological stability compared with compound 5h (**2**). Our process of development of lead compounds included the introduction of fluorine atoms into the inhibitor molecules to increase the binding affinity for the pocket of M^{pro} and the cell membrane permeability, and the replacement of the unstable amide bond by surrogates such as a thioamide structure. As a result, several potent inhibitors were developed through detailed structure–activity relationships focused on the P3, P2, P1, and P1′ sites of compound 5h (**2**). Compound **3** effectively blocks SARS-CoV-2 infection *in vitro* without significant cytotoxicity. Similar to compound 5h (**2**), compound **3** forms a covalent bond with the side chain thiol of the Cys145 residue of M^{pro} and according to the X-ray crystal structure analysis, enjoys hydrogen bond interactions and hydrophobic interactions with amino acid residues in the active site pocket of M^{pro}. Compound **3** also has highly potent enzymatic inhibitory activity against M^{pro} at the IC_{50} value of 0.037 ± 0.0010 µM. This is true of the other selected hit compounds, which have significant anti-SARS-CoV-2 activity in cells and possess remarkable enzymatic inhibitory activity, showing that there is a positive correlation between anti-SARS-CoV-2 activity and the enzymatic inhibitory activity against M^{pro}. Compound **3** showed one-order higher antiviral activity than 5h (**2**) and PF-07321332 (**1**), even in the EC_{99} values. Compound **3** exhibits high antiviral activity against several mutant strains such as QHN001 (α), TY8-612 (β), TY7-501 (γ), K1734 (δ), K5356 (κ), and 00012 (o, BA.1), and 02037 (o, BA.2) strains as against a WK-521 strain (ancestral Wuhan strain). This universal effectivity is the strong point of compound **3**. In future, the justification of testing compound **3** against SARS-CoV-2 variants would be expanded for plausible conquest of drug resistance to these M^{pro} inhibitors,[49,50] and the possible mutation in M^{pro} to confer viral evasion of known M^{pro} inhibitors, Nirmatrelvir/PF-07321332 (**1**) and 5h (**2**), was investigated in detail.[51] Furthermore, compound **4**, which has a thioamide structure in place of the amide bond between the P2 and P1 sites of compound **3**, has remarkable
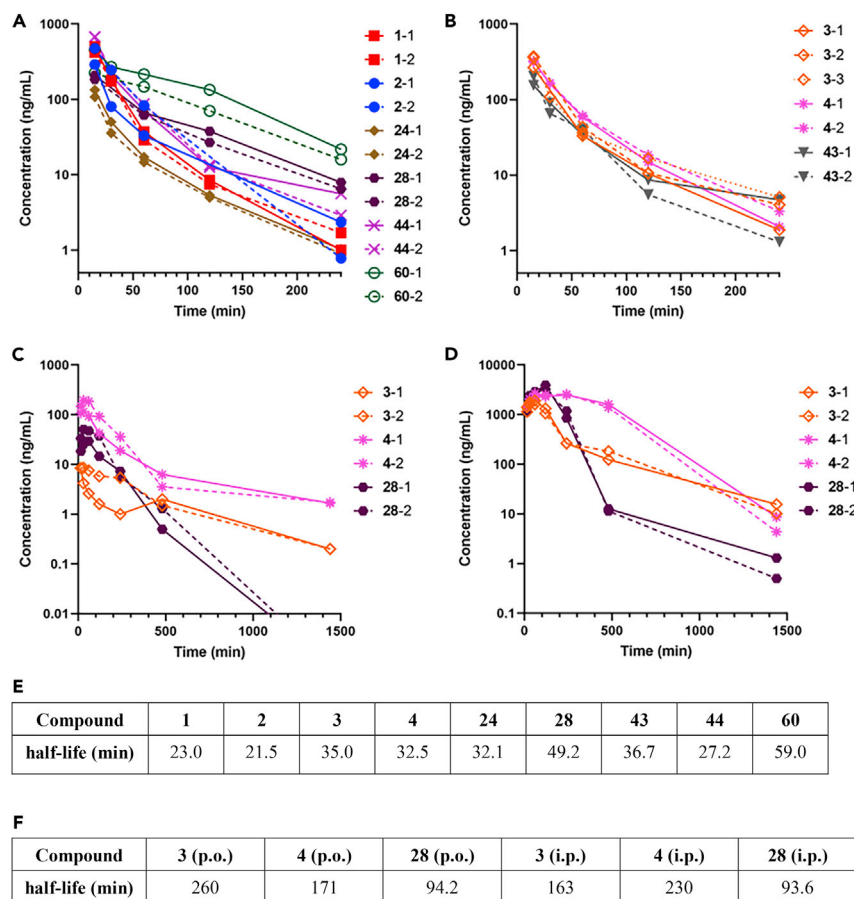
Figure 13. PK profiles of synthesized compounds in the mouse blood

(A–D) Plots of concentrations of synthesized compounds in the mouse blood after administration. (A) i.v. administration of compounds PF-07321332 (1), 5h (2), 24, 60, 44, and 28 at 2.0 mg/kg into mice; (B) i.v. administration of compounds 3, 4, and 43 at 2.0 mg/kg into mice; (C) p.o. administration of compounds 3, 4, and 28 at 20 mg/kg into mice; (D) i.p. administration of compounds 3, 4, and 28 at 20 mg/kg into mice. number: mouse number, ex. 1-1 and 1-2: two different mice with administration of compound 1.

(E and F) Calculated values of the half-lives (min) of the test compounds in i.v. administration (E, 240 min) and in p.o. and i.p. administrations (F, 1,440 min) from each data points in (A)–(D).

anti-SARS-CoV-2 activity, comparable with that of compound 3 in terms of EC_{50} and EC_{75} values, although the enzymatic inhibitory activity of compound 4 against M^{pro} is significantly lower than that of compound 3. Thus, thioamide derivatives might express significant activity in cells in proportion and relative to enzyme inhibitory activity, possibly because of enhanced cell membrane permeability or biological stability compared with the corresponding parent amide-type compounds. Significantly, compound 4 showed remarkably preferable pharmacokinetics in mice, especially in p.o. and i.p. administrations, compared with the corresponding parent compound 3, suggesting that replacement of the hydrolyzable amide bond by its thioamide surrogate structure can increase the biostability of the compound. Our data show that compounds 3 and 4 are useful drug candidates for M^{pro} inhibitors, and further development based on these compounds is continuing.

Limitations of the study

We have developed highly potent M^{pro} inhibitors that block SARS-CoV-2 infection *in vitro* without viral breakthrough. Some compounds showed remarkably preferable pharmacokinetics in mice compared with the parent compounds. Future experiments should evaluate the antiviral activity of these compounds in animal models of SARS-CoV-2 infection, and develop more effective inhibitors for drugs treating COVID-19 based on the present data.

iScience
Article

STAR★METHODS

Detailed methods are provided in the online version of this paper and include the following:

- KEY RESOURCES TABLE
- RESOURCE AVAILABILITY
  - Lead contact
  - Materials availability
  - Data and code availability
- EXPERIMENTAL MODEL AND SUBJECT DETAILS
  - Cells, viruses and test compounds
- METHOD DETAILS
  - Compound synthesis
  - Anti-SARS-CoV-2 assay and cytotoxicity assay
  - SARS-CoV-2 M^{pro} inhibition assays
  - Crystallization of M^{pro} and compound 3
  - Pharmokinetics investigations
- QUANTIFICATION AND STATISTICAL ANALYSIS

SUPPLEMENTAL INFORMATION

Supplemental information can be found online at https://doi.org/10.1016/j.isci.2022.105365.

AUTHOR CONTRIBUTIONS

#K.T., T.I., and T.K. contributed equally to the study.

K.T., T.I., T.K, N.H.-K., C.A., M.N., T.O., H.N., N.W., M.H., K.S., Y.M., T.K., S.H., N.T., N.K., T.O., K.N.: investigation; H.H., H.B., D.D., J.S.: analysis; S.M., H.M., H.T.: supervision; K.T., T.I., T.K., H.T.: writing.

All authors have given approval to the final version of the manuscript.

DECLARATION OF INTERESTS

The authors declare no competing interests.

REFERENCES

1. Zhu, N., Zhang, D., Wang, W., Li, X., Yang, B., Song, J., Zhao, X., Huang, B., Shi, W., Lu, R., et al. (2020). A novel coronavirus from patients with pneumonia in China, 2019. N. Engl. J. Med. *382*, 727–733. https://doi.org/10.1056/NEJMoa2001017.

2. Mitsuya, H., and Kokudo, N. (2020). Sustaining containment of COVID-19: global sharing for pandemic response. Glob. Health Med. *2*, 53–55. https://doi.org/10.35772/ghm.2020.01040.

3. Livingston, E., and Bucher, K. (2020). Coronavirus disease 2019 (COVID-19) in Italy. JAMA *323*, 1335. https://doi.org/10.1001/jama.2020.4344.

4. Li, Q., Guan, X., Wu, P., Wang, X., Zhou, L., Tong, Y., Ren, R., Leung, K.S.M., Lau, E.H.Y., Wong, J.Y., et al. (2020). Early transmission dynamics in Wuhan, China, of novel coronavirus-infected pneumonia. N. Engl. J. Med. *382*, 1199–1207. https://doi.org/10.1056/NEJMoa2001316.

5. Lopez Bernal, J., Andrews, N., Gower, C., Gallagher, E., Simmons, R., Thelwall, S., Stowe, J., Tessier, E., Groves, N., Dabrera, G., et al. (2021). Effectiveness of Covid-19 vaccines against the B.1.617.2 (delta) variant.

N. Engl. J. Med. *385*, 585–594. https://doi.org/10.1056/NEJMoa2108891.

6. Marcec, R., Majta, M., and Likic, R. (2021). Will vaccination refusal prolong the war on SARS-CoV-2? Postgrad. Med. J. *97*, 143–149. https://doi.org/10.1136/postgradmedj-2020-138903.

7. Pardo, J., Shukla, A.M., Chamarthi, G., and Gupte, A. (2020). The journey of Remdesivir: from Ebola to COVID-19. Drugs Context *9*, 2020–2024. https://doi.org/10.7573/dic.2020-4-14.

8. U.S. Food & Drug Administration. FDA approves first treatment for COVID-19. https://www.fda.gov/news-events/pressannouncements/fda-approves-first-treatment-covid-19.

9. Merck (2021). Merck and Ridgeback's Investigational Oral Antiviral Molnupiravir Reduced the Risk of Hospitalization or Death by Approximately 50% Compared to Placebo for Patients with Mild or Moderate COVID-19 in Positive Interim Analysis of Phase 3 Study (Merck & Co., Inc.).

10. World Health Organization. WHO updates its treatment guidelines to include molnupiravir. https://www.who.int/news/item/03-03-2022-molnupiravir.

11. McIntosh, J.A., Benkovics, T., Silverman, S.M., Huffman, M.A., Kong, J., Maligres, P.E., Itoh, T., Yang, H., Verma, D., Pan, W., et al. (2021). Engineered ribosyl-1-kinase enables concise synthesis of molnupiravir, an antiviral for COVID-19. ACS Cent. Sci. *7*, 1980–1985. https://doi.org/10.1021/acscentsci.1c00608.

12. Owen, D.R., Allerton, C.M.N., Anderson, A.S., Aschenbrenner, L., Avery, M., Berritt, S., Boras, B., Cardin, R.D., Carlo, A., Coffman, K.J., et al. (2021). An oral SARS-CoV-2 M^pro inhibitor clinical candidate for the treatment of COVID-19. Science *374*, 1586–1593. https://doi.org/10.1126/science.abl4784.

13. Hilgenfeld, R. (2014). From SARS to MERS: crystallographic studies on coronaviral proteases enable antiviral drug design. FEBS J. *281*, 4085–4096. https://doi.org/10.1111/febs.12936.

14. Muramatsu, T., Kim, Y.-T., Nishii, W., Terada, T., Shirouzu, M., and Yokoyama, S. (2013). Autoprocessing mechanism of severe acute respiratory syndrome coronavirus 3C-like protease (SARS-CoV 3CL^pro) from its polyproteins. FEBS J. *280*, 2002–2013. https://doi.org/10.1111/febs.12222.

15. Li, C., Qi, Y., Teng, X., Yang, Z., Wei, P., Zhang, C., Tan, L., Zhou, L., Liu, Y., and Lai, L. (2010). Maturation mechanism of severe acute respiratory syndrome (SARS) coronavirus 3C-like proteinase. J. Biol. Chem. *285*, 28134–28140. https://doi.org/10.1074/jbc.M109.095851.

16. Lindner, H.A., Fotouhi-Ardakani, N., Lytvyn, V., Lachance, P., Sulea, T., and Ménard, R. (2005). The papain-like protease from the severe acute respiratory syndrome coronavirus is a deubiquitinating enzyme. J. Virol. *79*, 15199–15208. https://doi.org/10.1128/JVI.79.24.15199-15208.2005.

17. Barretto, N., Jukneliene, D., Ratia, K., Chen, Z., Mesecar, A.D., and Baker, S.C. (2005). The papain-like protease of severe acute respiratory syndrome coronavirus has deubiquitinating activity. J. Virol. *79*, 15189–15198. https://doi.org/10.1128/JVI.79.24.15189-15198.2005.

18. Ghosh, A.K., Xi, K., Grum-Tokars, V., Xu, X., Ratia, K., Fu, W., Houser, K.V., Baker, S.C., Johnson, M.E., and Mesecar, A.D. (2007). Structure-based design, synthesis, and biological evaluation of peptidomimetic SARS-CoV 3CLpro inhibitors. Bioorg. Med. Chem. Lett. *17*, 5876–5880. https://doi.org/10.1016/j.bmcl.2007.08.031.

19. Hattori, S.I., Higashi-Kuwata, N., Hayashi, H., Allu, S.R., Raghavaiah, J., Bulut, H., Das, D., Anson, B.J., Lendy, E.K., Takamatsu, Y., et al. (2021). A small compound with an indole moiety inhibits the main protease of SARS-CoV-2 and blocks virus replication. Nat. Commun. *12*, 668. https://doi.org/10.1038/s41467-021-20900-6.

20. Unoh, Y., Uehara, S., Nakahara, K., Nobori, H., Yamatsu, Y., Yamamoto, S., Maruyama, Y., Taoda, Y., Kasamatsu, K., Suto, T., et al. (2022). Discovery of S-217622, a noncovalent oral SARS-CoV-2 3CL protease inhibitor clinical candidate for treating COVID-19. J. Med. Chem. *65*, 6499–6512. https://doi.org/10.1021/acs.jmedchem.2c00117.

21. Hoffman, R.L., Kania, R.S., Brothers, M.A., Davies, J.F., Ferre, R.A., Gajiwala, K.S., He, M., Hogan, R.J., Kozminski, K., Li, L.Y., et al. (2020). Discovery of ketone-based covalent inhibitors of coronavirus 3CL proteases for the potential therapeutic treatment of COVID-19. J. Med. Chem. *63*, 12725–12747. https://doi.org/10.1021/acs.jmedchem.0c01063.

22. Qiao, J., Li, Y.-S., Zeng, R., Liu, F.-L., Luo, R.-H., Huang, C., Wang, Y.-F., Zhang, J., Quan, B., Shen, C., et al. (2021). SARS-CoV-2 M^pro inhibitors with antiviral activity in a transgenic mouse model. Science *371*, 1374–1378. https://doi.org/10.1126/science.abf1611.

23. Bai, B., Belovodskiy, A., Hena, M., Kandadai, A.S., Joyce, M.A., Saffran, H.A., Shields, J.A., Khan, M.B., Arutyunova, E., Lu, J., et al. (2022). Peptidomimetic α-acyloxymethylketone warheads with six-membered lactam P1 glutamine mimic: SARS-CoV-2 3CL protease inhibition, coronavirus antiviral activity, and in vitro biological stability. J. Med. Chem. *65*, 2905–2925. https://doi.org/10.1021/acs.jmedchem.1c00616.

24. Xia, Z., Sacco, M., Hu, Y., Ma, C., Meng, X., Zhang, F., Szeto, T., Xiang, Y., Chen, Y., and Wang, J. (2021). Rational design of hybrid SARS-CoV-2 main protease inhibitors guided by the superimposed cocrystal structures with the peptidomimetic inhibitors GC-376, telaprevir, and boceprevir. ACS Pharmacol. Transl. Sci. *4*, 1408–1421. https://doi.org/10.1021/acsptsci.1c00099.

25. Ma, C., Xia, Z., Sacco, M.D., Hu, Y., Townsend, J.A., Meng, X., Choza, J., Tan, H., Jang, J., Gongora, M.V., et al. (2021). Discovery of di- and trihaloacetamides as covalent SARS-CoV-2 main protease inhibitors with high target specificity. J. Am. Chem. Soc. *143*, 20697–20709. https://doi.org/10.1021/jacs.1c08060.

26. Wang, H., Pei, R., Li, X., Deng, W., Xing, S., Zhang, Y., Zhang, C., He, S., Sun, H., Xiao, S., et al. (2022). The structure-based design of peptidomimetic inhibitors against SARS-CoV-2 3C like protease as Potent anti-viral drug candidate. Eur. J. Med. Chem. *238*, 114458. https://doi.org/10.1016/j.ejmech.2022.114458.

27. Ma, Y., Yang, K.S., Geng, Z.Z., Alugubelli, Y.R., Shaabani, N., Vatansever, E.C., Ma, X.R., Cho, C.-C., Khatua, K., Xiao, J., et al. (2022). A multi-pronged evaluation of aldehyde-based tripeptidyl main protease inhibitors as SARS-CoV-2 antivirals. Eur. J. Med. Chem. *240*, 114570. https://doi.org/10.1016/j.ejmech.2022.114570.

28. Thanigaimalai, P., Konno, S., Yamamoto, T., Koiwai, Y., Taguchi, A., Takayama, K., Yakushiji, F., Akaji, K., Chen, S.E., Naser-Tavakolian, A., et al. (2013). Development of potent dipeptide-type SARS-CoV 3CL protease inhibitors withNovel P3 scaffolds: design, synthesis, biological evaluation, and docking studies. Eur. J. Med. Chem. *68*, 372–384. https://doi.org/10.1016/j.ejmech.2013.07.037.

29. Konno, S., Thanigaimalai, P., Yamamoto, T., Nakada, K., Kakiuchi, R., Takayama, K., Yamazaki, Y., Yakushiji, F., Akaji, K., Kiso, Y., et al. (2013). Design and synthesis of new tripeptide-type SARS-CoV 3CL protease inhibitors containing an electrophilic arylketone moiety. Bioorg. Med. Chem. *21*, 412–424. https://doi.org/10.1016/j.bmc.2012.11.017.

30. Konno, S., Kobayashi, K., Senda, M., Funai, Y., Seki, Y., Tamai, I., Schäkel, L., Sakata, K., Pillaiyar, T., Taguchi, A., et al. (2022). 3CL protease inhibitors with an electrophilic arylketone moiety as anti-SARS-CoV-2 agents. J. Med. Chem. *65*, 2926–2939. https://doi.org/10.1021/acs.jmedchem.1c00665.

31. Zhou, P., Zou, J., Tian, F., and Shang, Z. (2009). Fluorine bonding — how does it work in protein−ligand interactions? J. Chem. Inf. Model. *49*, 2344–2355. https://doi.org/10.1021/ci9002393.

32. Gillis, E.P., Eastman, K.J., Hill, M.D., Donnelly, D.J., and Meanwell, N.A. (2015). Applications of fluorine in medicinal chemistry. J. Med. Chem. *58*, 8315–8359. https://doi.org/10.1021/acs.jmedchem.5b00258.

33. Shah, P., and Westwell, A.D. (2007). The role of fluorine in medicinal chemistry. J. Enzym. Inhib. Med. Chem. *22*, 527–540. https://doi.org/10.1080/14756360701425014.

34. Smart, B.E. (2001). Fluorine substituent effects (on bioactivity). J. Fluor. Chem. *109*, 3–11. https://doi.org/10.1016/S0022-1139(01)00375-X.

35. Schweizer, E., Hoffmann-Röder, A., Schärer, K., Olsen, J.A., Fäh, C., Seiler, P., Obst-Sander, U., Wagner, B., Kansy, M., and Diederich, F. (2006). A fluorine scan at the catalytic center of thrombin: C–F, C–OH, and

C–OMe bioisosterism and fluorine effects on pK_a and log D values. ChemMedChem *1*, 611–621. https://doi.org/10.1002/cmdc.200600015.

36. Morgenthaler, M., Aebi, J.D., Grüninger, F., Mona, D., Wagner, B., Kansy, M., and Diederich, F. (2008). A fluorine scan of non-peptidic inhibitors of neprilysin: fluorophobic and fluorophilic regions in an enzyme active site. J. Fluor. Chem. *129*, 852–865. https://doi.org/10.1016/j.jfluchem.2008.02.004.

37. Hyohdoh, I., Furuichi, N., Aoki, T., Itezono, Y., Shirai, H., Ozawa, S., Watanabe, F., Matsushita, M., Sakaitani, M., Ho, P.-S., et al. (2013). Fluorine scanning by nonselective fluorination: enhancing Raf/MEK inhibition while keeping physicochemical properties. ACS Med. Chem. Lett. *4*, 1059–1063. https://doi.org/10.1021/ml4002419.

38. Giroud, M., Harder, M., Kuhn, B., Haap, W., Trapp, N., Schweizer, W.B., Schirmeister, T., and Diederich, F. (2016). Fluorine scan of inhibitors of the cysteine protease human cathepsin L: dipolar and quadrupolar effects in the π-stacking of fluorinated phenyl rings on peptide amide bonds. ChemMedChem *11*, 1042–1047. https://doi.org/10.1002/cmdc.201600132.

39. Meanwell, N.A. (2018). Fluorine and fluorinated motifs in the design and application of bioisosteres for drug design. J. Med. Chem. *61*, 5822–5880. https://doi.org/10.1021/acs.jmedchem.7b01788.

40. Ghosh, A.K., Rao, K.V., Nyalapatla, P.R., Kovela, S., Brindisi, M., Osswald, H.L., Sekhara Reddy, B., Agniswamy, J., Wang, Y.-F., Aoki, M., et al. (2018). Design of highly potent, dual-acting and central-nervous-system-penetrating HIV-1 protease inhibitors with excellent potency against multidrug-resistant HIV-1 variants. ChemMedChem *13*, 803–815. https://doi.org/10.1002/cmdc.201700824.

41. Bulut, H., Hattori, S.I., Aoki-Ogata, H., Hayashi, H., Das, D., Aoki, M., Davis, D.A., Rao, K.V., Nyalapatla, P.R., Ghosh, A.K., and Mitsuya, H. (2020). Single atom changes in newly synthesized HIV protease inhibitors reveal structural basis for extreme affinity, high genetic barrier, and adaptation to the HIV protease plasticity. Sci. Rep. *10*, 10664. https://doi.org/10.1038/s41598-020-65993-z.

42. Hattori, S.I., Hayashi, H., Bulut, H., Rao, K.V., Nyalapatla, P.R., Hasegawa, K., Aoki, M., Ghosh, A.K., and Mitsuya, H. (2019). Halogen bond interactions of novel HIV-1 protease inhibitors (PI) (GRL-001-15 and GRL-003-15) with the flap of protease are critical for their potent activity against wild-type HIV-1 and multi-PI-resistant variants. Antimicrob. Agents Chemother. *63*, 02635-18. https://doi.org/10.1128/AAC.02635-18.

43. Chen, X., Mietlicki-Baase, E.G., Barrett, T.M., McGrath, L.E., Koch-Laskowski, K., Ferrie, J.J., Hayes, M.R., and Petersson, E.J. (2017). Thioamide substitution selectively modulates proteolysis and receptor activity of therapeutic peptide hormones. J. Am. Chem. Soc. *139*, 16688–16695. https://doi.org/10.1021/jacs.7b08417.

44. Phan, H.A.T., Giannakoulias, S.G., Barrett, T.M., Liu, C., and Petersson, E.J. (2021). Rational design of thioamide peptides as selective inhibitors of cysteine protease cathepsin L. Chem. Sci. *12*, 10825–10835. https://doi.org/10.1039/d1sc00785h.

45. Schless, J.M., Allison, R.F., Inglis, R.M., White, E.F., and Topperman, S. (1965). The use of ethionamide in combined drug regimens in the re-treatment of isoniazid resistant pulmonary tuberculosis. Am. Rev. Respir. Dis. *91*, 728–737. https://doi.org/10.1164/arrd.1965.91.5.728.

46. Liu, C., Barrett, T.M., Chen, X., Ferrie, J.J., and Petersson, E.J. (2019). Fluorescent probes for studying thioamide positional effects on proteolysis reveal insight into resistance to cysteine proteases. Chembiochem *20*, 2059–2062. https://doi.org/10.1002/cbic.201900115.

47. Shalaby, M.A., Grote, C.W., and Rapoport, H. (1996). Thiopeptide synthesis. α-Amino thionoacid derivatives of nitrobenzotriazole as thioacylating agents. J. Org. Chem. *61*, 9045–9048. https://doi.org/10.1021/jo961245q.

48. Dragovich, P.S., Prins, T.J., Zhou, R., Webber, S.E., Marakovits, J.T., Fuhrman, S.A., Patick, A.K., Matthews, D.A., Lee, C.A., Ford, C.E., et al. (1999). Structure-based design, synthesis, and biological evaluation of irreversible human rhinovirus 3C protease inhibitors. 4. Incorporation of P1 lactam moieties as l-glutamine replacements. J. Med. Chem. *42*, 1213–1224. https://doi.org/10.1021/jm9805384.

49. Ullrich, S., Ekanayake, K.B., Otting, G., and Nitsche, C. (2022). Main protease mutants of SARS-CoV-2 variants remain susceptible to nirmatrelvir. Bioorg. Med. Chem. Lett. *62*, 128629. https://doi.org/10.1016/j.bmcl.2022.128629.

50. Hu, Y., Lewandowski, E.M., Tan, H., Morgan, R.T., Zhang, X., Jacobs, L.M.C., Butler, S.G., Mongora, M.V., Choy, J., Chen, Y., et al. (2022). Naturally occurring mutations of SARS-CoV-2 main protease confer drug resistance to nirmatrelvir. Preprint at bioRxiv. https://doi.org/10.1101/2022.06.28.497978.

51. Yang, K.S., Leeuwon, S.Z., Xu, S., and Liu, W.R. (2022). Evolutionary and structural insights about potential SARS-CoV-2 evasion of nirmatrelvir. J. Med. Chem. *65*, 8686–8698. https://doi.org/10.1021/acs.jmedchem.2c00404.

52. Shirato, K., Nao, N., Katano, H., Takayama, I., Saito, S., Kato, F., Katoh, H., Sakata, M., Nakatsu, Y., Mori, Y., et al. (2020). Development of genetic diagnositic methods for novel coronavirus 2019 (nCoV-2019) in Japan. Jpn. J. Infect. Dis. *73*, 304–307. https://doi.org/10.7883/yoken.JJID.2020.061.

53. Anson, B.J., Chapman, M.E., Lendy, E.K., Pshenychnyi, S., D'Aquila, R.T., Satchell, K.J.F., and Mesecar, A.D. (2020). Broad-spectrum inhibition of coronavirus main and papainlike proteases by HCV drugs. Res. Square. https://doi.org/10.21203/rs.3.rs-26344/v1.

54. Hirata, K., Yamashita, K., Ueno, G., Kawano, Y., Hasegawa, K., Kumasaka, T., and Yamamoto, M. (2019). ZOO: an automatic data-collection system for high-throughput structure analysis in protein microcrystallography. Acta Crystallogr. D Struct. Biol. *75*, 138–150. https://doi.org/10.1107/S2059798318017795.

55. Winter, G., Waterman, D.G., Parkhurst, J.M., Brewster, A.S., Gildea, R.J., Gerstel, M., Fuentes-Montero, L., Vollmar, M., Michels-Clark, T., Young, I.D., et al. (2018). *DIALS*: implementation and evaluation of a new integration package. Acta Crystallogr. D Struct. Biol. *74*, 85–97. https://doi.org/10.1107/S2059798317017235.

56. Vagin, A., and Teplyakov, A. (2010). Molecular replacement with *MOLREP*. Acta Crystallogr. D Biol. Crystallogr. *66*, 22–25. https://doi.org/10.1107/S0907444909042589.

57. Murshudov, G.N., Skubák, P., Lebedev, A.A., Pannu, N.S., Steiner, R.A., Nicholls, R.A., Winn, M.D., Long, F., and Vagin, A.A. (2011). *REFMAC5* for the refinement of macromolecular crystal structures. Acta Crystallogr. D Biol. Crystallogr. *67*, 355–367. https://doi.org/10.1107/S0907444911001314.

58. Schüttelkopf, A.W., and van Aalten, D.M.F. (2004). *PRODRG*: a tool for high-throughput crystallography of protein-ligand complexes. Acta Crystallogr. D Biol. Crystallogr. *60*, 1355–1363. https://doi.org/10.1107/S0907444904011679.

59. Higashi-Kuwata, N., Hayashi, S., Kumamoto, H., Ogata-Aoki, H., Das, D., Venzon, D., Hattori, S.I., Bulut, H., Hashimoto, M., Otagiri, M., et al. (2021). Identification of a novel long-acting 4′-modified nucleoside reverse transcriptase inhibitor against HBV. J. Hepatol. *74*, 1075–1086. https://doi.org/10.1016/j.jhep.2020.12.006.

60. Jaki, T., and Wolfsegger, M.J. (2011). Estimation of pharmacokinetic parameters with the R package PK. Pharmaceut. Statist. *10*, 284–288. https://doi.org/10.1002/pst.449.

STAR★METHODS

KEY RESOURCES TABLE

REAGENT or RESOURCE	SOURCE	IDENTIFIER
Antibodies		
primary antibodies: convalescent IgG fraction	a convalescent COVID-19 individual, reference S1	N/A
secondary antibody: goat polyclonal anti-human-IgG-Alexa Fluor 488 Fab fragment antibody	Jackson ImmunoResearch Laboratories, Inc	Cat#109-547-003; RRID: AB_2337854
Texas Red™-X dye conjugated Phalloidin	Thermo Fisher Scientific	Cat#T7471
Bacterial and virus strains		
JPN/TY/WK-521 (SARS-CoV-2^{WK-521})	National Institute of Infectious Diseases (Tokyo, Japan)	GISAID Accession ID; EPI_ISL_408667
B.1.1.7 (alpha) strain [hCoV-19/Japan/QHN001/2020 (SARS-CoV-2^{QHN001})]	clinically isolated, National Institute of Infectious Diseases	GISAID Accession ID; EPI_ISL_804007)
B.1.351 (beta) strain [hCoV-19/Japan/TY8-612-P0/2021 (SARS-CoV-2$^{TY8-612}$)]	clinically isolated, National Institute of Infectious Diseases	GISAID Accession ID; EPI_ISL_1123289
P.1 (gamma) strain [hCoV-19/Japan/TY7-501-P0/2021 (SARS-CoV-2$^{TY7-501}$)]	clinically isolated, National Institute of Infectious Diseases	GISAID Accession ID; EPI_ISL_833366
B.1.617.2 (delta) strain [hCoV-19/Japan/TKYK01734/2021 (SARS-CoV-2^{K1734})]	clinically isolated, Tokyo Metropolitan Institute of public Health	GISAID Accession ID; EPI_ISL_2080609
B.1.617.1 (kappa) strain [TKYTK5356_2021 (SARS-CoV-2^{5356})]	clinically isolated, Tokyo Metropolitan Institute of public Health	GISAID Accession ID; EPI_ISL_2378733
BA.1.1.529 (omicron BA.1) strain [hCoV-19/Japan/TKYX00012/2021 (SARS-CoV-2^{000129})]	clinically isolated, Tokyo Metropolitan Institute of public Health	GISAID Accession ID; EPI_ISL_8559478
BA.1.1.529 (omicron BA.2) strain [hCoV-19/Japan/TKYS02037/2022 (SARS-CoV-2^{02037})]	clinically isolated, Tokyo Metropolitan Institute of public Health	GISAID Accession ID; EPI_ISL_9397331
Biological samples		
BL21-CodonPlus(DE3)-RIL strain	Agilent	Cat#230245
Chemicals, peptides, and recombinant proteins		
SARS-CoV-2 M^{pro}/3CL^{pro}	Hattori et al.[19]	Accession #: MN908947
Nirmatrelvir	MedChemExpress	HY-138687
Remdesivir	Selleck	S8932
Critical commercial assays		
3CL Protease, Untagged (SARS-CoV-2) Assay Kit	BPS Bioscience	Cat#78042-1
QIAamp Viral RNA Mini QIAcube Kit	Qiagen	Cat#52926
One Step PrimeScript III RT-qPCR mix	TaKaRa Bio	Cat# RR600B
Cell Counting Kit-8	Dojindo	Cat# 341-08001
Deposited data		
SARS-CoV-2 M^{pro}-compound **3** co-crystal structure	This paper	PDB: 8DOY
Experimental models: Cell lines		
VeroE6 cell	ATCC https://www.atcc.org/products/crl-1586	Cat# ATCC CRL-1586

(Continued on next page)

CellPress
OPEN ACCESS

Continued

REAGENT or RESOURCE	SOURCE	IDENTIFIER
Experimental models: Organisms/strains		
Jcl:ICR (ICR) female mice	CLEA Japan	Cat# Jcl:ICR https://www.clea-japan.com/products/outbred/item_a0340
Oligonucleotides		
5'-AAATTTTGGGGACCAGGAAC-3' (forward)	SARS-CoV-2 nucleocapsid	Shirato et al.[52]
5'- TGGCAGCTGTGTAGGTCAAC-3' (reverse)	SARS-CoV-2 nucleocapsid	Shirato et al.[52]
5'-FAM-ATGTCGCGCATTGGCATGGA-black hole quencher 1 (BHQ1)-3'	SARS-CoV-2 nucleocapsid	Shirato et al.[52]
Recombinant DNA		
pGEX-4T1 vector (cloned into SARS-CoV2 M^{pro}-encoding sequence)	https://www.genscript.com/	The sequence of SARS-CoV 3CL Protease was optimized and synthesized at GensSript and cloned into PGEX-4T1 vectors for *E. Coli expression*
Software and algorithms		
QuantAnalysis Ver2.2.1	Bruker Daltonics	Cat#1836735
R software (version 4.0.5)	R Foundation for Statistical Computing	https://www.r-project.org/
MolRep	Vagin and Teplyakov[56]	https://www.ccp4.ac.uk/html/molrep.html
REFMAC5	Murshudov et al.[57]	https://www2.mrc-lmb.cam.ac.uk/groups/murshudov/
Dundee PRODRG2 server	Schüttelkopf and van Aalten[58]	http://davapc1.bioch.dundee.ac.uk/cgi-bin/prodrg
ChemDraw Professional 18.0	PerkinElmer	https://www.perkinelmer.com/category/chemdraw
GraphPad Prism 9	GraphPad	https://www.graphpad.com/scientific-software/prism/
Other		
preparative HPLC: JASCO PU-2086 plus/UV-2075 plus	JASCO Corporation	https://www.jasco.co.jp/jpn/product/index.html#LC
preparative HPLC: JASCO PU-2087 plus/UV-2075 plus	JASCO Corporation	https://www.jasco.co.jp/jpn/product/index.html#LC
preparative HPLC: JASCO PU-4086-Binary/UV-4075	JASCO Corporation	https://www.jasco.co.jp/jpn/product/index.html#LC
analytical HPLC: JASCO PU-2089 plus/UV-2075 plus	JASCO Corporation	https://www.jasco.co.jp/jpn/product/index.html#LC
automatic silica gel flash column chromatography system (Isolera One)	Biotage	https://www.biotage.com/isolera-1-flash-chromatography-instrument
Pure C-815	Buchi	https://www.buchi.com/en/products/instruments/pure-chromatography-systems
NMR: Bruker AVANCE III 400 spectrometer	Bruker Daltonics	https://www.bruker.com/en/products-and-solutions/mr/nmr.html
NMR: Bruker AVANCE 500	Bruker Daltonics	https://www.bruker.com/en/products-and-solutions/mr/nmr.html
NMR: JNM-ECA500	JEOL	https://www.jeol.co.jp/en/products/category_nmr.html
SPring-8 BL41XU	SPring-8	http://www.spring8.or.jp/wkg/BL41XU/instrument/lang-en/INS-0000000328?set_language=en&cl=en

(Continued on next page)

CellPress
OPEN ACCESS

iScience
Article

Continued		
REAGENT or RESOURCE	SOURCE	IDENTIFIER
MS: micrOTOF focus	Bruker Daltonics	https://www.bruker.com/en/products-and-solutions/mass-spectrometry.html
LC-MS/MS: impact II	Bruker Daltonics	https://www.bruker.com/en/products-and-solutions/mass-spectrometry.html

RESOURCE AVAILABILITY

Lead contact

Further information and requests for resources should be directed to and will be fulfilled by Hirokazu Tamamura (tamamura.mr@tmd.ac.jp).

Materials availability

This study did not generate new materials or reagents.

Data and code availability

Data reported in this article will be shared by the lead contact on request. The data of the X-ray crystallographic analysis of the co-crystal structure of SARS-CoV-2 M^{pro} and compound **3** were deposited into the PDB under the ID: 8DOY. Any additional information required to reanalyze the data reported in this article is available from the lead contact on request. Structural representation of X-ray co-crystal structures of SARS-CoV-2 M^{pro} and 5h/**3**, immunostaining experimental data, PK data, X-ray data set and synthetic procedures were provided as Figures S1–S3, Tables S1 and S2 and Data S1 (PDF).

EXPERIMENTAL MODEL AND SUBJECT DETAILS

Cells, viruses and test compounds

VeroE6 cells were obtained from the ATCC (Manassas, VA, USA) and were maintained in Dulbecco's modified Eagle's medium (D-MEM) supplemented with 10% fetal bovine serum (FBS), 100 μg/mL of penicillin, and 100 μg/mL of streptomycin. SARS-CoV-2 strain JPN/TY/WK-521 (SARS-CoV-2^{WK-521}) was obtained from the National Institute of Infectious Diseases (Tokyo, Japan). Five clinically isolated SARS-CoV-2 mutant strains were used in the current study: a B.1.1.7 (alpha) strain [hCoV-19/Japan/QHN001/2020 (SARS-CoV-2^{QHN001}, GISAID Accession ID; EPI_ISL_804007)], a B.1.351 (beta) strain [hCoV-19/Japan/TY8-612-P0/2021 (SARS-CoV-2$^{TY8-612}$)] and a P.1 (gamma) strain [hCoV-19/Japan/TY7-501-P0/2021 (SARS-CoV-2$^{TY7-501}$)] were obtained from National Institute of Infectious Diseases, Tokyo, Japan. A B.1.617.2 (delta) strain [hCoV-19/Japan/TKYK01734/2021 (SARS-CoV-2^{K1734}, GISAID Accession ID; EPI_ISL_2080609)], a B.1.617.1 (kappa) strain [TKYTK5356_2021 (SARS-CoV-2^{5356}, DDBJ Accession ID; LC633761)], a BA.1.1.529 (omicron BA.1) strain [hCoV-19/Japan/TKYX00012/2021 (SARS-CoV-2^{00012}, GISAID Accession ID; EPI_ISL_8559478)] and a BA.1.1.529 (omicron BA.2) strain [hCoV-19/Japan/TKYS02037/2022 (SARS-CoV-2^{02037}, GISAID Accession ID; EPI_ISL_9397331)] were provided from Tokyo Metropolitan Institute of public Health, Tokyo, Japan. Each variant was shown to contain each VOC-specific amino acid substitutions before the assays conducted in the present study (*vide infra*). An antiviral agent Nirmatrelvir (**1**) (PF-07321332)[12] was purchased from MedChemExpress (Monmouth Junction, NJ). 5h (**2**) was synthesized by Arun K. Ghosh (Purdue University, USA).[21] Remdesivir[7,8] was purchased from Selleck (Sylvanfield Drive, Houston). Each compound was dissolved in DMSO at 20 mM as stock solutions.

METHOD DETAILS

Compound synthesis

The synthetic methods for representative compounds **3** and **4** are described in Figures 2 and 3. The purity of all of the final compounds, measured by analytical HPLC or NMR is >95%. Experimental procedures including characterization data are provided in Data S1.

Anti-SARS-CoV-2 assay and cytotoxicity assay

For antiviral assay, cells were seeded in a 96-well plate (2×10^4 cells/well) and incubated. After 1 day, virus was inoculated into cells at each multiplicity of infection (MOI): SARS-CoV-2^{WK-521}, 0.33; SARS-CoV-2^{QHN001}(alpha),

iScience
Article

CellPress
OPEN ACCESS

25; SARS-CoV-2TY8-612(beta), 25; SARS-CoV-2[TY7-501] (gamma), 20; SARS-CoV-2[K1734] (delta), 20; SARS-CoV-2[K5356] (kappa), 20; SARS-CoV-2[00012] (omicron BA.1), 32; SARS-CoV-2[02037] (omicron BA.2), 33. After additional 3 days, cell culture supernatants were harvested and viral RNA was extracted using a QIAamp viral RNA minikit (Qiagen, Hilden, Germany), and quantitative RT-PCR (RT-qPCR) was then performed using One Step PrimeScript III RT-qPCR mix (TaKaRa Bio, Shiga, Japan) following the instructions of the manufacturers. The primers and probe used for detecting SARS-CoV-2 nucleocapsid[52] were 5′-AAATTTTGGGGACCAGGAAC-3′ (forward), 5′- TGGCAGCTGTGTAGGTCAAC-3′ (reverse), and 5′-FAM-ATGTCGCGCATTGGCATGGA-black hole quencher 1 (BHQ1)-3′ (probe). To determine the cytotoxicity of each compound, cells were seeded in a 96-well plate (2×10^4 cells/well). One day later, various concentrations of each compound were added, and cells were then incubated for additional 3 days. The 50% cytotoxic concentrations (CC_{50}) values were determined using the WST-8 assay and Cell Counting Kit-8 (Dojindo, Kumamoto, Japan).

SARS-CoV-2 M^{pro} inhibition assays

The inhibitory activity (IC_{50}) of each compound against M^{pro} was determined using 3CL Protease, Untagged (SARS-CoV-2) Assay Kit (BPS Bioscience: Catalog#: 78042-1). SARS-CoV-2 M^{pro}/3CL^{pro} (Accession #: MN908947) with the authentic *N*- and *C*-terminal residues that are released after cleavage from the polyprotein was used for all assays. The details for expression and purification of this fully active M^{pro} construct was described.[53] In general, inhibition of M^{pro} by a test compound was assessed using a continuous fluorescence assay and the FRET-based substrate UIVT3 (HiLyte Fluor488 TM–ESATLQSGLRKAK-QXL520 TM-NH_2) (Anaspec, Fremont, CA). The assay buffer consisted of 50 mM HEPES pH 7.50, 0.1 mg/mL BSA, 0.01% Triton X-100, 2 mM DTT, 1% DMSO and a final enzyme concentration of 200 nM. The assays were performed in Costar 3694 EIA/RIA 96-well half-area, flat bottom, black polystyrene plates (Corning, Corning, NY) at 25 °C. The increase in fluorescence intensity of M^{pro} catalyzed reactions was measured at a wavelength of 528 nm (20 nm bandwidth) using an excitation wavelength of 485 nm (bandwidth 20 nm) using either a CLARIOstar Plate Reader (BMG Labtech, Cary, NC) or a Synergy H1 hybrid multi-mode plate reader (BioTek, Winooski, VT). The Relative Fluorescence Units (RFU) was measured and plotted to calculate IC_{50} values.[19]

Crystallization of M^{pro} and compound 3

The M^{pro} solution was concentrated to 3 mg/mL and incubated with 300 µM of **3** for 1 h before crystallization. Crystals were grown using a hanging drop vapour diffusion method at 20 °C. The reservoir solution contained 0.1 M MES pH 6.0, 15% polyethyene glycol (PEG) 6000 and 3% DMSO. Crystals were soaked briefly in a cryoprotection solution containing 0.1 M MES pH 6.0, 35% PEG 400 and 5% DMSO. X-ray data were collected at SPring-8 BL41XU (Hyogo, Japan) using the automatic data collection system ZOO[54] and processed by DIALS using xia2 incorporated in ccp4i2.[55] The source wavelength for the data collection was 1.0 Å. Data collection statistics are shown in SI, Table S1. The phase problem was solved by molecular replacement using MolRep[56] using the 2.16 Å structure of M^{pro} (PDB: 6LU7 or 7JKV) as a model. All water molecules and ligand atoms were omitted from the starting model. Subsequent cycles of refinement to 1.25 Å resolution were performed in REFMAC5.[57] Structure file of compound **3** was generated using the Dundee PRODRG2 server[58] and manually fitted to the electron density. All structural figures were produced with MOE (ver. 2020.0901). The data were deposited into the PDB under the PDB: 8DOY.

Pharmokinetics investigations

Animal experiments[59]

Jcl:ICR (ICR) female mice were purchased from CLEA Japan (Tokyo, Japan). A test compound was administrated by intravenous (2 mg/kg), intraperitoneal (20 mg/kg) or oral (20 mg/kg) injection to ICR mice with body weights ranging from 20 to 30 g (n = 2 or 3). At various time points after administration (i.v.: 15, 30, 60, 120 and 240 min; i.p., p.o.: 0.25, 0.5, 1, 2, 4, 8 and 24 h), blood samples were collected from the retro-orbital venous plexus under sevoflurane anesthesia and centrifuged at 3,000 rpm for 15 min to obtain plasma.

All mice were housed in an air-conditioned animal room at 23 ± 2 °C with a relative humidity of 40–60% under specific pathogen-free conditions, with a 12 h light/dark cycle (08:00−20:00/20:00−08:00). All mice were fed a standard rodent CE-2 diet (CLEA Japan) and had *ad libitum* access to water. All animal experiments were approved by the President of the National Center for Global Health and Medicine (NCGM) following consideration by the Institutional Animal Care and Use Committee of the NCGM

(approval ID no. 21057) and were carried out in accordance with institutional procedures, national guidelines, and the relevant national laws on the protection of animals.

Sample preparation for LC-MS/MS

5 μL of plasma samples was added to 20 μL of MeCN and kept at 4 °C for 15 min for protein precipitation. After centrifugation, the obtained supernatant was added to TFA to give a final concentration of 0.05% for LC-MS/MS analysis.

LC-MS/MS analysis

To quantify the compounds in prepared samples for LC-MS/MS, analysis was done using a quadrupole-time-of-flight (QTOF) mass spectrometer equipped with a Captive Spray electrospray ionization platform in the positive mode (impact II, Bruker Daltonics, Bremen, Germany) with liquid chromatography (Ultimate 3000 HPLC, Thermo Fisher Scientific, MA). An injected sample was concentrated on an Acclaim PepMap100 C18 trap column (Thermo Fisher Scientific) at flow rate of 20 μL/min. For sample separation, reverse-phase chromatography was conducted using an Acclaim PepMap100 C18 LC column (0.075 mm × 150 mm, 2 μm particle) (Thermo Fisher Scientific) in conditions of isocratic mode of 95% MeCN and 0.1% formic acid for 7 min, a flow rate of 300 nL/min and a temperature of 35 °C. Multiple reaction monitoring mode was used in LC-MS/MS analysis and quantitative analysis was performed by using QuantAnalysis Ver2.2.1 (Bruker Daltonics). A non-compartment model was used for the pharmacokinetic analysis. Each parameter was calculated using the R software (version 4.0.5, R Foundation for Statistical Computing, Vienna, Austria) with the "PK" package.[60]

QUANTIFICATION AND STATISTICAL ANALYSIS

Numbers represent the average IC_{50} value $\pm$ SD (μM), EC_{50} value $\pm$ SD (μM), and CC_{50} value $\pm$ SD (μM) from two independent experiments. A non-compartment model was used for the pharmacokinetic analysis, and each parameter was calculated using the R software (version 4.0.5, R Foundation for Statistical Computing, Vienna, Austria) with the "PK" package.[60]